Stefan Stauder, B.Sc.

Behaviour of a novel algorithm for fragmentation analysis based on 3D images from photogrammetry

MASTER'S THESIS

Submitted in fulfilment of the requirements for the degree of

Diplom-Ingenieur

Master's programme Geotechnical and Hydraulic Engineering

at

Graz University of Technology

Supervisors

O.Univ.-Prof. Dipl.-Ing. Dr.mont. Wulf Schubert

Institut für Felsmechanik und Tunnelbau

Technische Universität Graz

Andreas Buyer, B.Sc. M.Sc.

Institut für Felsmechanik und Tunnelbau

Technische Universität Graz

Dipl.-Ing. Dr.techn. Markus Pötsch

3GSM GmbH

Dipl.-Ing. Matthias Wimmer, Ph.D.

LKAB

Graz, September 2018

Affidavit

Ich erkläre an Eides statt, dass ich die vorliegende Arbeit selbstständig verfasst, andere als die angegebenen Quellen/Hilfsmittel nicht benutzt und die den benutzten Quellen wörtlich und inhaltlich entnommenen Stellen als solche kenntlich gemacht habe. Das in TUGRAZonline hochgeladene Textdokument ist mit der vorliegenden Masterarbeit identisch.

I declare that I have authored this thesis independently, that I have not used others than the declared sources/resources and that I have explicitly marked all material which has been quoted either literally or by content from the used sources. The text document uploaded to TUGRAZonline is identical to the present master‘s thesis.

Datum / Date

Unterschrift / Signature

Principle of equality

Due to reasons of legibility, this work does not include gender-specific formulations. However, the used male expressions stand for both genders.

Danksagung

An dieser Stelle möchte ich mich bei all jenen bedanken, die mich bereits während meiner Studienzeit unterstützt und mir bei der Fertigstellung dieser Arbeit geholfen haben.

Besonderer Dank gilt auch meinen Betreuern Andreas Buyer, Markus Pötsch und Matthias Wimmer, welche mir ermöglicht haben diese Arbeit zu verfassen und mir auch in stressigen Situationen immer mit Rat und Tat zu Seite gestanden sind. Weiters möchte ich Herrn Prof. Wulf Schubert danken, dessen Vorlesungen mein Interesse am Tunnelbau geweckt haben.

Dankeschön auch allen Wegbegleitern des Stahlbauzeichensaals. Ohne die Gemeinschaft, die intensiven Lernwochenenden und natürlich den Spaß bei den anschließenden Feiern, wäre mein Studium wohl nur halb so schön gewesen.

Mein größter Dank gilt allerdings meiner Familie. Danke Mama für die unermüdliche Unterstützung in allen Lebenslagen, danke Oma und Opa, dass ihr mich so oft in Graz besucht habt. Dabei konntet ihr ja nicht nur Graz kennenlernen, sondern auch so einige interessante Einblicke in den WG-Alltag gewinnen. Zum Schluss möchte ich mich noch bei meiner Freundin Bianca bedanken, die mir seit ich sie kennenlernen durfte, jeden Tag abseits des Studiums zu einem besonderen gemacht hat (Danke an dieser Stelle natürlich auch an ihren Bruder, dem ich diesen Umstand verdanke).

Abstract

Sublevel Caving (SLC) is used as a mining method in the LKAB underground mines in Kiruna (Sweden). Fragmentation in SLC is vitally important and effects almost every branch of modern mining operations. Reliable, quick and non-invasive measurement of the fragmentation is a key premise for successful research and development work, as well as a smooth mining routine.

Currently, an autonomous full-scale fragmentation measurement system does not exist. Various 2D and 3D algorithms have not yet managed to solve the numerous problems and fulfil the requirements. Therefore, LKAB initiated with 3GSM GmbH the development of a novel image-based algorithm to measure the fragmentation. The approach starts from 3D digital surface models, determines the particle borders by curvature analysis and improves the results by using 2D image processing.

This thesis is intended to test the algorithm's features. Starting with the delineation evaluation of selected examples, continuing with the comparison of the algorithm's results with muck piles with known fragment size distribution and finally, applying the algorithm to real muck pile data from the Kiruna underground mine. All calculations were conducted with alpha-level software packages and, for the sake of clarity, post-processed.

Kurzfassung

Die Erzgewinnung in den Bergwerken der LKAB in Kiruna (Schweden) erfolgt hauptsächlich in Form von "Sublevel Caving" (SLC). Dabei spielt die Zerkleinerung des Rohmaterials eine tragende Rolle. Die Zerkleinerung beeinflusst fast alle Teilbereiche eines modernen Abbaubetriebs. Eine verlässliche, schnelle und nicht-invasive Messung der Zerkleinerung ist die Grundlage sowohl für eine erfolgreiche Forschung und Entwicklung, als auch einen reibungslosen Untertagebau.

Ein dearartiges autonomes Messsystem existiert allerdings derzeit nicht. Diverse 2D bzw. 3D Algorithmen konnten die umfangreichen Anforderungen bis jetzt nicht zufriedenstellend erfüllen. Aus diesem Grund regte die LKAB zusammen mit der Firma 3GSM GmbH, die Entwicklung eines neuen fotogrammetrie-basierten Zerkleinerungsalgorithmus an, welcher die Krümmung von möglichen Fragmenten auf Grund eines digitalen Oberflächenmodells bestimmt und diese, mit Hilfe von 2D Bildverarbeitung, ergänzt.

Diese Masterarbeit hat den Zweck, die Grundfunktionen des neu entwickelten Algorithmus zu testen. Im ersten Schritt wird die Kornabgrenzung an ausgewählten Beispielen ausgewertet, anschließend werden bekannte Sieblinien mit den Ergebnissen des Algorithmus verglichen und schlussendlich erfolgt die Auswertung der Korngrößenverteilungen tatsächlicher Haufwerke des Untertagebaus in Kiruna. Alle Berechnungen wurden mit Hilfe von alpha-level Softwarepaketen durchgeführt und zur besseren Übersicht nachbearbeitet.

Contents

List of Figures

List of Tables

1 Introduction

1.1 Background

Sublevel caving (SLC) is used as a mining method in the LKAB underground mines in Kiruna (Sweden). Fragmentation in SLC is vitally important. It affects both, the gravity flow of broken rock and any downstream processes. Reliable measurement of the fragmentation is a key premise for successful research and development work, especially if gravity flow is analyzed in detail or operative changes are necessary.
Currently, there is still no reliable full-scale fragmentation measurement system available. Both, 2D and 3D algorithms are obviously not flawless yet. For this reason, LKAB initiated together with 3GSM GmbH the development of a coupled 2D/3D image based fragmentation algorithm. The main difference of the proposed approach to previous ones is that analysis starts in 3D from the surface geometry, determines particle borders by curvature analysis of the surface and improves the results by using 2D image information from known methods, e.g. gradient images for edge detection.

1.2 Thesis objectives and structure

The newly developed fragmentation algorithm has to be thoroughly tested. Based on laboratory tests and full-scale data, the output should be verified by analysis of muck piles (artificial and real) with known Fragment Size Distributions (FSD), to find a range of optimum program settings, reducing false detections and flawed results. A comparison with the 2D algorithm software Split-Desktop (Split Engineering, 2010) is conducted in a subsequent report, to determine the status quo and the benefit of the investigated measurement approach and is therefore not included in the present thesis.

This thesis is intended to establish the newly designed algorithm for fragmentation analysis and bases on the following research questions:

1. Is the fragment delineation plausible regarding the number of false positives and true negatives?
2. Withstands the obtained FSD of the algorithm a verification by known grading curves from artificial muck piles?
3. What are the software's limitations at the current state and what is possible regarding the 3D fragmentation algorithm in the future?

The thesis is divided into five chapters. In Chapter 1, a short introduction of the problem statement is given. The objectives and structure of this work are declared and general terms of interest as SLC and fragmentation are explained. Further on in Chapter 2, the latest developments containing 2D and 3D image analysis regarding fragmentation are discussed (State of the Art). Chapter 3 explains the used method to acquire plausible results like image pre-processing, 3D fragmentation analysis and the laboratory apparatus, with instrumentation and techniques, applied in various tests. The results from the laboratory and full scale tests are illustrated in Chapter 4. Chapter 5 discusses the results regarding accuracy in particle delineation and sizing, by means of visual inspection and a comparison with known grading curves. The conclusions are presented in Chapter 6 along with answers to the thesis's elementary questions. Finally, the on-going work at the fragmentation algorithm and recommendations on further research, related to full-scale or laboratory experimental testing, are discussed and possible suggestions for improvement of the newly developed software are given.

1.3 Sublevel caving

Sublevel caving is a mass mining method based upon the utilization of gravity flow of blasted ore and caved waste rock (Kvapil, 1998). It is a productive method, where all of the ore is fragmented by blasting, while the overlying host rock fractures and caves under the action of mine induced stresses and gravity. The temporary void created by ore extraction is filled by caved waste originating from the overlying rock mass. SLC was initially applied in the early 1900s to extract soft iron ores found in Minnesota and Michigan. Back then, heavily timbered drift support was sequentially removed at the end of a drift, which lead to caving

and slushing out of the ore. When dilution got too big, the next set of timbers was removed, etcetera (Cokayne, 1982). Today, many uncertainties about fragmentation and ore cavability are eliminated due to drilling and blasting from drifts on successive sublevels. The long hole drillings in ring patterns and the opening race are carried out after the production drives are fully excavated and reinforced. Mining the ore by blasting leads to a rather fracture and joint independent extraction process of the rock mass, compared to other comparable mining methods. SLC is usually carried out, when open pit mining is uneconomic and is nowadays usually applied in hard, strong ore in which the hanging wall progressively caves, keeping pace with the retreating rings. It is suitable for large ore bodies with a steep dip. Due to caving of waste rock into the blasted ore, a certain degree of ore loss and waste rock dilution cannot be avoided. Additionally, caving can also cause subsidence on the surface (www-1, 2018).

The excavation is performend by drill and blast at several stages as illustrated in Figure 1.1. The SLC geometry consits of a series of sublevels created at intervals in between 20 and 30 m beginning at the top and working downwards.

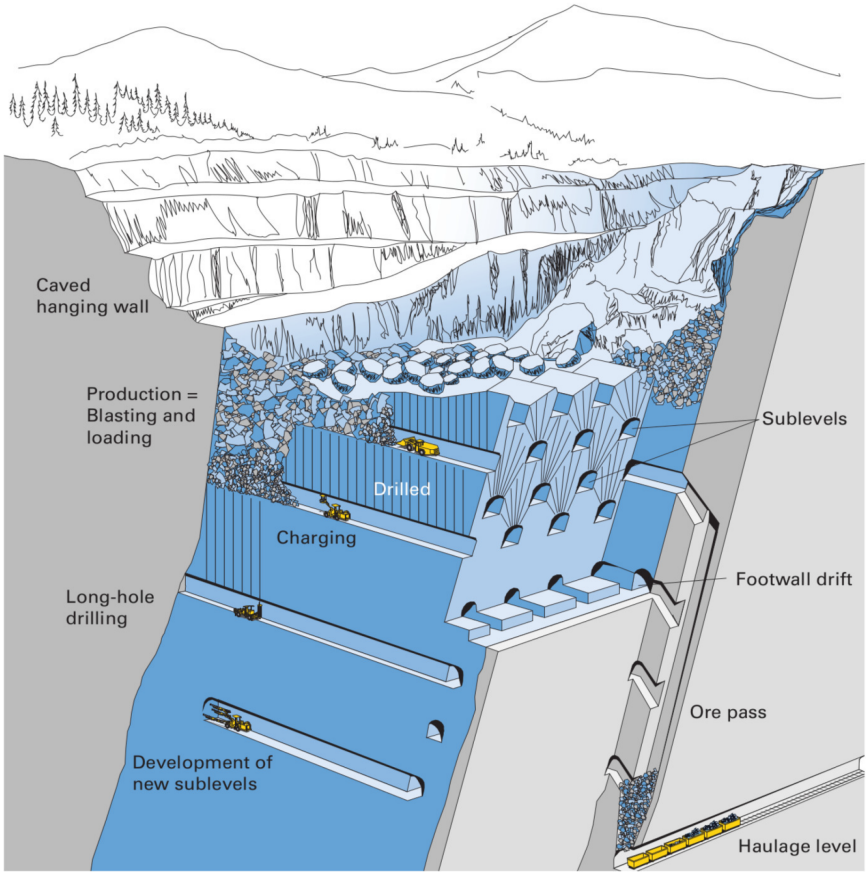

Figure 1.1: Modern SLC layout in 3D (© Atlas Copco).

To quarry the ore, underground transportation routes (drifts) are excavated. Development drifts are blasted parallel, directly through the ore body, on each sublevel with drifts being offset sideways between the different sublevels. Reinforcement, if necessary, consists of bolts, mesh and sprayed concrete.

From each drift, boreholes are drilled upwards through the ore body in a fan-shaped pattern (fan cut, Figure 1.1). A new draw point is exposed closest to the hanging wall by an opening blast. After contact with the overlying levels is established, the rings are blasted subsequently. The distance between two consecutive rings, called burden, is about two to three metres. The extraction of ore from one blasted ring continues, until dilution or an other specified characteristic reaches a crucial level. If so, the next ring is blasted and the process repeats.

After blasting is completed, the iron ore is removed from the drifts by underground loaders. The ore is tipped into vertical shafts, called ore passes. Herein, the ore falls due to gravity and is collected in rock bins just above the main level (haulage level).

Afterwards, the ore must be transported from those rock bins at the ore pass to the crushers by autonomous trains or trucks. Here, the crushers break the ore into pieces with a diameter of about ten centimetres. The broken fragments are then transported on conveyor belts to the skip hoists, which transport the material to the surface (www-2, 2018). In Figure 1.2 a visualisation of the SLC method is illustrated.

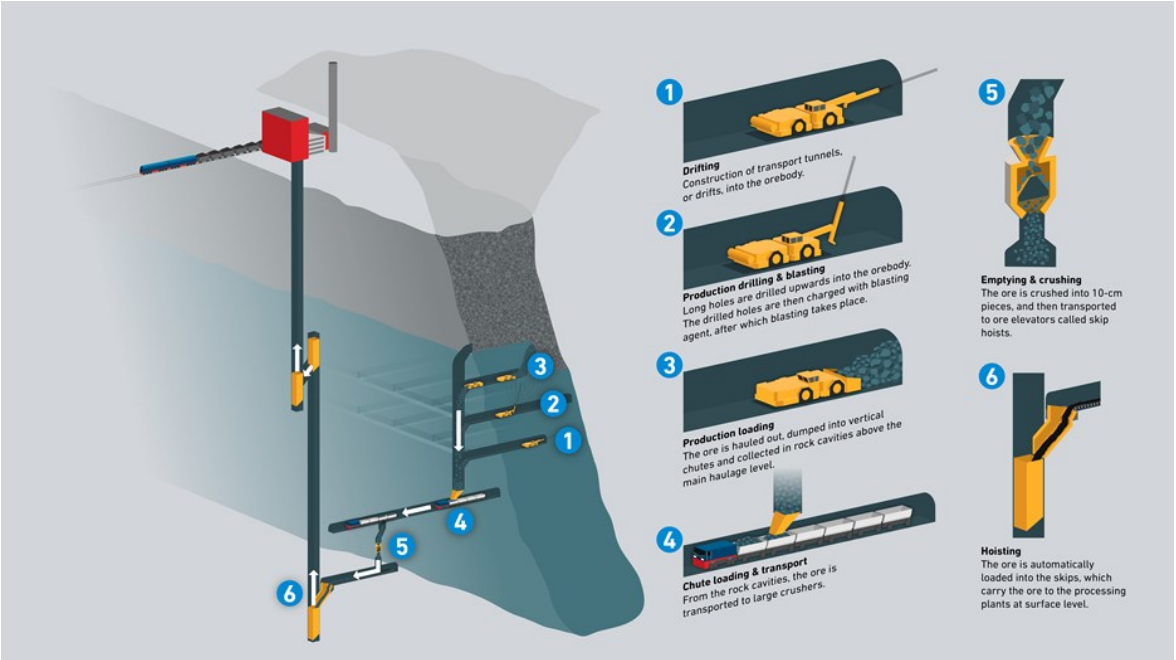

Figure 1.2: SLC exemplified (© LKAB).

1.4 Fragmentation and Fragment Size Distribution

The extent to which a rock mass is broken into small pieces is called fragmentation. Fragmentation is primarily controlled by mechanical tools as blasting, caving and draw of rock or ore in situ and hydraulic fracturing. Secondary impacts are breakage due to loading and transportation of the mined material to the crushers (Rustan et al., 2011b). There are various influencing factors on the fragmentation outcome like the drilling performance, the charging of the borehole, the rock mass properties, the caving masses and also human factors (Table 1.1).

Table 1.1: Influences on fragmentation due to SLC (Wimmer, 2017)

Drilling	Diameter, burden, spacing, ring inclination
Charging	Explosives, timing, specific charge
Rock mass properties	Stresses, number of joint sets, joint set properties and orientation
Caving masses	Confinement of blastfront, compaction capacity (void ratio)
Human factors	Experience

The knowledge about the fragmentation of the blasted material can be used to adjust and optimize the influencing parameters given (Table 1.1) which have a direct impact on the loading-, hauling-, crushing- and milling- efficiency at an underground mine. Not only the fragmentation of the rock mass itself is important, but also the FSD in muck piles plays an important role regarding post-processing of the blasted material. The requirements for the FSD are very complex and many factors have to be taken into account. Main deliberations are made regarding:

- The percentage of fines with almost no depth spread (draw bodies) after removing the first buckets.
- Too coarse-grained material possibly leads to hang-ups during the removal and in the ore pass.
- The Load-Haul-Dump (LHD) performance (ideal fragmentation for quick charging of the bucket and low wear).
- Additional costs and wear of equipment for post-processing (hydraulic hammering) of boulder-sized blocks.

The FSD is defined as the relationship between the cumulative amount of fragments in percent passing a specific mesh size and the mesh size (Rustan et al., 2011a). Figure 1.3 shows an example of a FSD gathered by 3D image analysis.

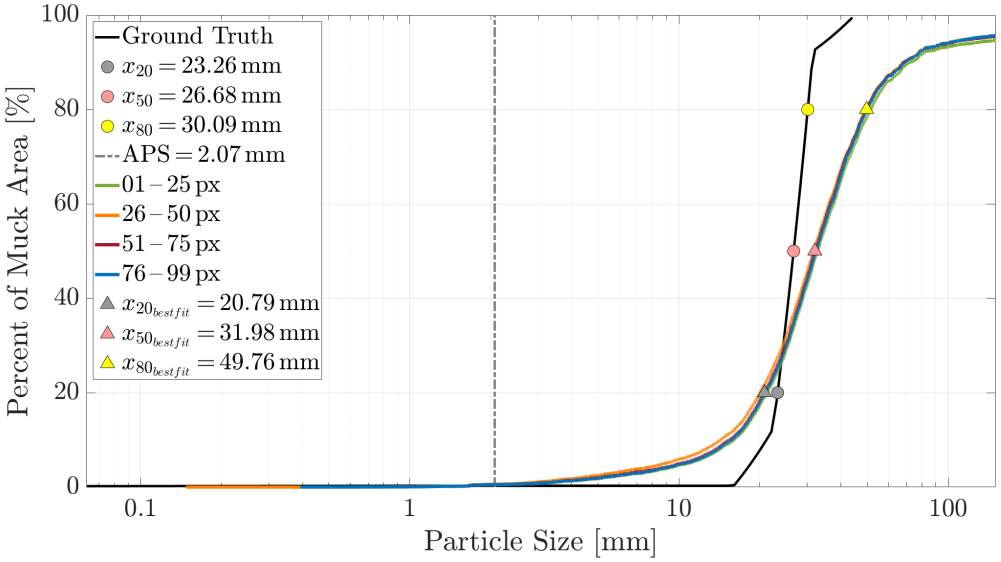

Figure 1.3: Example of a FSD.

The best way to obtain a FSD, which resembles the actual fragmentation, is by sieving the buckets. However, this is very time consuming and leads, considering the scale of the fragmented ore/rock mixture, to an enormous increase of the mining expenses. As a result, sieving is conducted only in intervals by the LKAB research and development department. Currently, the rock fragmentation size analysis software Split-Desktop is used on regular basis to determine the FSD. Split-Desktop is a 2D image-based analysis software, using image processing for the particle delineation.

2 State of the Art

2.1 2D image analysis

The advantages of gathering the fragment size distribution in muck piles via image processing are obvious. Image processing is fast, inexpensive, compared to actual sieving and does not interfere with the production. With the development of cheaper hardware and improved analyses algorithms, digital image processing is a substantial help in research fields together with the mining industry (Rhigetti, 2014). Some of the benefits of the optical fragmentation analysis over sieving are:

- The measurement is quick, conducted semi-automatically and eliminates human subjectivity. This eases a quick adaptation of the production to the in situ conditions.
- The analysis is conducted parallel to the production without interference of the ongoing mining work.
- Due to the inexpensive and fast processing of the images many samples can be analyzed. This reduces the significance of sampling errors drastically.
- Due to the large volume of fragmented rock, actual sieving is only conducted at stated intervals for occasional research work. Image processing on the other hand has no restrictions in volume for analysis.
- Optical analysis is non-destructive and decreases tool wear and the handling of material to a minimum. Only the image acquisition system must be elaborated and maintained frequently (Maerz et al., 1996).

Despite the development and great improvements of optical measuring systems over the past years, sources of errors are inherent. It is obvious, that only visually apparent features can be measured to a certain extent. Consequently, the accuracy of the results is controlled by resolution, light exposure and the position between camera and muck pile. Furthermore,

the images have to be rectified and scaled, to allow metric measurements. Sources of errors regarding the 2D image analysis could be classified according to Maerz & Zhou (1998) as follows.

2.1.1 Confining factors of 2D image analysis

In the following subsections, several factors, influencing either the particle delineation in 2D or their sizing are described.

Colour, texture and resolution

Colour and texture highly influence the delineation. The edge detection algorithm, which is based on difference in contrast between neighbouring pixels, could interpret particle borders wrong. The contrast along the muck pile surface is controlled by lighting variability and shadowing. Variable or uneven lightning can lead to blurry contrast conditions resulting in a poor delineation. This factor goes hand in hand with the image quality. Eden & Franklin (1996) differ between two possible outcomes of poor delineation in terms of block misidentification: disintegration and fusion. Disintegration is defined as a separation of a large fragment into smaller ones due to misinterpretation of the fragment edges. The opposite of this phenomena is called fusion, where the algorithm fails to recognise block boundaries and misdetects various smaller fragments as one block.
Another problem is that most image processing software is not able to identify and delineate sub-pixel sized particles. Those fragments, fines, are not detected and can lead to an overestimation of the mean fragment size distribution, if not classified manually in a post-processing step (Rhigetti, 2014).

Unfolding model

Optical 2D measuring systems gather the block area or cross section in two dimensions. To model the fragmentation more realistically, some systems like Split-Desktop transform this 2D information into a 3D space, called unfolding. Those volume interpretations involve assumptions about the particle shape, the possible fragment overlap and an estimation of the depth spread of non-visible particles (Sanchidrián et al., 2008). To minimize the errors from inadequate unfolding, those need to be eliminated by extensive and empirical calibration. Otherwise the computed FSD is scaled wrong.

2.1.2 Sample presentation

Fragment orientation

Maerz & Zhou (1998) state the following hypothesis: assuming anisotropic block shapes and blocks laying primarily flat on the pile's surface, imaging systems will tend to measure the major and intermediate axis of the block. However, sieves theoretically measure the minor and intermediate axis. Basing the analysis on bigger dimensions leads to a larger particle area, shifting the FSD to the right towards bigger fragment sizes. This phenomena is called overestimation of the FSD.

Overlapping fragments

In a muck pile, individual fragments are typically overlapped by other particles. This is indifferent in sieving, because every block is evaluated individually by the sequence of sieves. In contrast, it is difficult to delineate and classify overlapping fragments. The influence of this problem can be reduced by using an appropriate unfolding model.

2.1.3 Imaging process

Variable lighting and perspective

The lighting of the muck pile has a direct impact on the amount of the delineation error. Most 2D fragmentation software's edge detection algorithm responds to shadows between adjacent blocks. Hence, wrong lighting conditions can lead to both, disintegration and fusion of neighbouring fragments due to weak or inappropriate lighting.
Photos, not taken at a perpendicular angle to a preferable planar surface of the muck pile, can lead to optical distortion and affect the measurement of the fragment size.

Manual post-processing

So far, automatic delineation has not outdated manual post-processing. However, due to individual perception and experience, manual editing is subjective and not reproducible. In addition, the more time is spent on manual editing, the higher the accuracy of the results. An "optimized time", i.e. the minimum time needed to create the best possible analysis output,

with an acceptable relative error, should be determined (Rhigetti, 2014). Sanchidrián et al. (2005) investigated the operator influence on the manual delineation result and found, that the user dependency gets particularly visible at small scale fragments and the classification of fines, whereas at bigger fragment sizes, different operators provide almost the same result. Hence, the improvement of the results by manually classifying the insufficiently detected fines and smaller fragments is highly depended on the operator. This leads possibly to a statistical dispersion of the measurement.

2.1.4 Sampling

By taking a photo of particles with a probably wide spread FSD, it is hard to find an appropriate scale and location to represent all fragment sizes in one image. Some blocks may be too large to fit on one picture, whilst others are too small to be recognized at all. As an outcome, the FSD acquired by the optical system, could be very depended on the covered region of the muck pile. The more homogeneous the analyzed material is, the lower the influence of the sampling region gets. Sampling errors are considered to influence the FSD the most.
Despite the possible inaccuracies described above, another problem related to optical fragmentation measurement systems is the missing information regarding both, the depth spread of fragments and the fragment sizes below.
According to Rhigetti (2014), a typical muck pile contains block sizes over two or three orders of magnitude (10 to $10^{2\text{-}3}$). However, the order of a typical optical system is limited to 1 - 1.5. This means, particles smaller than $1/10^{1.5}$ of the biggest block are classified as fines and consequently not detected. This causes an overestimation of the FSD. Not only the resolution limits the fines delineation though. Altogether there are two possible reasons for missing fines:

1. The fines detection is limited by the imaging resolution.
2. Small fragments are located behind bigger fragments due to segregation.

The difficulty to detect fines is not yet overcome and so different fragmentation tools use different approaches to reduce the influence of this problem. For an example, Split-Desktop tries to compensate the missing fines during the unfolding process and completes the slope of the FSD below a certain cut-off value, where the resolution is too low, with a Schumann or Rosin-Rammler distribution (Split Engineering, 2016).

2.2 3D image analysis

There are few publications regarding fragmentation analysis by 3D imaging using photogrammetry. Still, the aim to improve the fragmentation result by adding the third dimension to the measurement, goes back as far as the late 1990s. Such systems however, didn't become available until more generic software for the PC was developed in the early to mid first decade of 2000. Back then it became possible to adapt photogrammetry software packages for other measurement purposes, like fragmentation analysis (Noy, 2013). Han & Song (2014) use stereo-imaging to extract the spatial information of a muck pile. This data is then used as an input parameter for the statistical estimation of the blasted fragments. In laboratory experiments, they compared the photogrammic and a 2D image processing approach (Split-Desktop) with water tank volume measurements. Thurley et al. (2015) undertook a fragmentation monitoring trial on 3D imaging of a draw-point and the corresponding bucket load of a LHD. The fragment delineation logic is based on edge detection using morphological operators and watershed segmentation.

The previous applications of 3D image analysis regarding fragmentation measurement described above, deliver a rough estimation of the actual grading curve, with remaining potential for improvements. As described, automated block detection has not yet outdated manual editing, which is subjective and not reproducible. To overcome this problems and the other mentioned shortcomings in section 2.1, a new method for determining the FSD is currently under development. This new approach combines a 3D surface and a 2D image analysis derived from a 3D image and shall lead to an improved estimation of the FSD in muck piles. It aims to minimize user interaction, manual post-processing and should provide an automated logic, robust to a variety of block sizes.

The used algorithm for the fragmentation analysis is integrated in the BlastMetriX Fragmenter (BMX Fragmenter). A 3D surface model generated by multiple photos, serves as input for the analysis.

2.2.1 Generation of a 3D surface model

A 3D surface model (3D image) is the combination of a set of photographic images and the spatial information of the observed object. Briefly, it connects the visual with the geometric information. The process starts by taking photos of the object of interest from different locations. Afterwards, a dense set of related image points is derived. The position and the

relative orientation of the cameras are recovered automatically from the associated image coordinates. A set of points in 3D (point cloud) is obtained by a spatial intersection of rays generated through the corresponding image points and the relative location (Figure 2.1). The final 3D image is the overlay of the digital photograph and the meshed surface between the point cloud (Gaich et al., 2010). The benefit of measuring real distances, areas and volumes at a 3D surface model is now used to obtain the FSD of a muck pile.

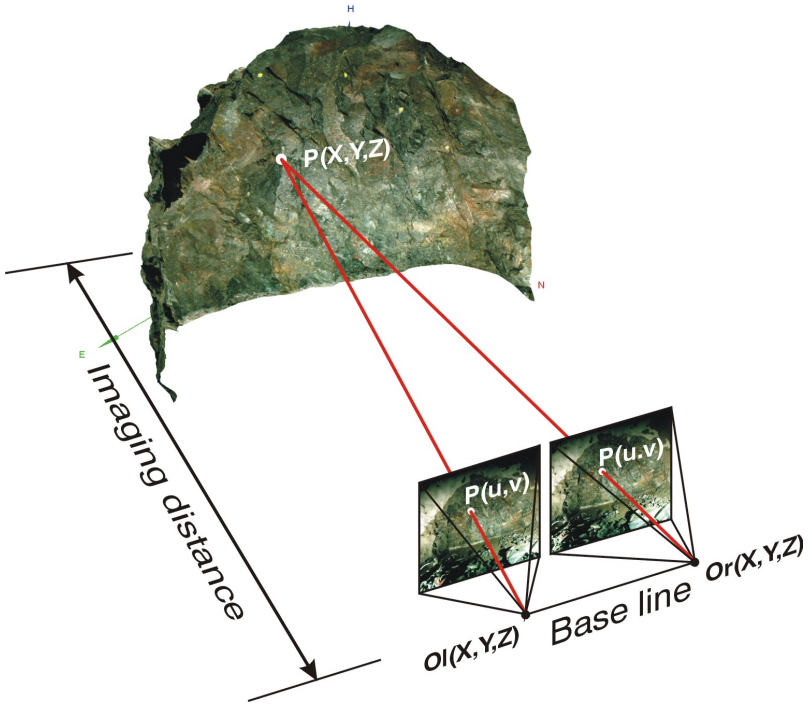

Figure 2.1: Schematic generation of a 3D image from a pair of photos (© 3GSM).

2.2.2 3D vs. 2D

By adding the spatial information to the analysis procedure, better approximations about the actual FSD at the muck pile's surface are expected. Additionally, the curvature evaluation of detected blocks and the ellipsoid fitting at a likeable fragment, could lead to a better understanding of a possible overlap between fragments and allows a little peek underneath the surface. Through the combination of 3D curvature analysis and traditional 2D image processing like morphological operations, texture analysis and color evaluation, the automatized fragment delineation of the BMX Framenter should lead to better and more reliable FSD without manual post-processing of the data.

2.2.3 Confining factors of 3D image analysis

Since this is the first test of the 3GSM fragmentation logic, it is difficult to estimate the limitations of the new algorithm. It is likely that some errors illustrated in section 2.1 can be reduced or even eliminated, but some problems will probably remain and undergo further investigation, when the software's version is in a further state.

Colour, texture and resolution

As colour and texture highly influence the delineation, adding curvature analysis of the muck pile surface should seriously support the edge detection algorithm, especially in regions of insufficient contrasts. Statements about disintegration and fusion are made in Chapter 5.
The sub-pixel size delineation is a physical problem and not expected to be solved.
To visualize the border between visible and not visible particles in the 3D image, thresholds for the ground sampling distance and the average point spacing are planned.

Unfolding model

Due to 3D modelling of the muck pile's surface from the scratch, unfolding is not needed and this source of error is eliminated.

2.2.4 Sample presentation

Fragment orientation and overlapping fragments

The fragment orientation plays an important role regarding the quality of the measured FSD by 3D analysis. As the BMX Fragmenter's logic uses the minor and intermediate axis of a fitted ellipsoid (see subsection 3.2.2) a better convergence rate between software and actual sieving is expected.
Statements about the benefit regarding the detection of overlapping fragments are hard to predict. As soon as the fragmentation algorithm is tested and the software is in a further state, a solution concerning the problem of fragment overlap could be pursued.

2.2.5 Imaging process

Variable lighting and perspective

Since the 3D surface model is computed by images, the lighting of the muck pile and the angle of photo acquisition relative to an imagined planar surface of the heap still has a direct impact on the amount of the delineation error in a 3D fragmentation analysis approach.

Manual post-processing

The main target of LKAB and 3GSM is to minimize user interaction and to speed up and automatize the data processing. Only regarding the tagging of fines areas, an user input is planned in the current software's state.

2.2.6 Sampling

Sampling will be a problem until camera's resolution take another great step forward to cover and represent all fragment sizes in a wide spread muck pile in just one picture. As long as the resolution stays the same, some blocks will continue to be too large to fit on one picture, whilst others are too small to be recognized at all.
Due to 3D imaging a limited prediction of the depth spread of fragments and the particle sizes below the surface is possible.

The algorithm's features for evaluating the fragmentation of a muck pile and the current software's version are described in Chapter 3.

3 Method

Selected data-sets of muck pile and LHD bucket photographs, taken at the Kiruna LKAB mine as well as in an Austrian limestone quarry, are used to generate 3D digital surface models (DSM), which are analyzed with the BMX Fragmenter. Each set is composed of at least two images, taken from fixed camera positions. The DSM are scaled and oriented with the known maximum camera distances and a manual selection of the ground floor orientation. The muck pile and the bucket filling from the Kiruna mine are well graded and heterogeneous, whereas the muck piles from the limestone quarry are both, homogeneous and closely graded as well heterogeneous and well graded. This chapter describes the workflow performed in this thesis.

3.1 Data basis and instrumentation

The image data and instrumentation, used for the image acquisition, is divided into an on-sight and a laboratory part. These sections differ in photograph origin and equipment usage.

3.1.1 Mine and laboratory data

As mentioned, the data includes "artificial" heaps with known FSD from an Austrian limestone quarry and "real" fragmented, blasted rock from the LKAB mine in Kiruna. The knowledge about the grading curve of the artificial muck pile is gathered by sieving. For the verification, the FSD must lie in the defined range with a confidence level of 95 %. On the contrary, there is no grading curve knwon from the LKAB heaps. The data with known ground truth is used for a thorough parameter study and their verification, whereas the real data serves for the performance evaluation. Table 3.1 presents the used 3D models involving the location of the gathered images, the model name, the properties of the muck pile according to optical appraisal and the purpose of usage are shown.

Table 3.1: Data basis for fragmentation analysis with the BMX Fragmenter.

Location	Model	Properties			Purpose
		Apperance	FSD	Color	
Graz	22_32_I	homog.	homog.	uniform	Study & verification
Graz	22_32_II	homog.	homog.	uniform	Study & verification
Graz	00_63_I	homog.	heterog.	uniform	Study & verification
Graz	00_63_II	heterog.	heterog.	uniform	Study & verification
Kiruna (front)	set_00	heterog.	unknown	uniform	Evaluation
Kiruna (bucket)	bucket_01	heterog.	unknown	uniform	Evaluation

3.1.2 Used cameras

To generate a 3D image from digital photos by the LKAB Central Control Routine (CCR), the shots have to be taken from at least two different positions. The distance between the pictures is known for scaling and the region of interest (ROI) must overlap 100 % on all images (see section 3.2). Again, a distinction must be made between the camera setup in Kiruna and the setup for laboratory testing in Graz, which are described in subsection 3.1.3. The image acquiring setup affects the requirements for the used cameras. The front-station setup in Kiruna is fixed at the crown of the drift and uses four different cameras, whereas the bucket-station has two cameras and takes two photos. The portable camera setup used in the limestone quarry is mounted on a slider. The testing system allows the usage of just one camera and can take any number of photos needed for the simulation. The used cameras are listed in Table 3.2. As the bucket data is provided as a DSM and not computed manually, the camera settings are not known.

Table 3.2: Camera setup for image acquisition.

Location	Camera & Objective			
	outer left	inner left	inner right	outer right
Graz	”	Canon EOS 70D Tamron AF 17-50 mm		”
Kiruna (front)	Nikon D90 Tamron AF 17-50 mm	Nikon D610 AF-S Nikkor 24-70 mm		Nikon D90 Tamron AF 17-50 mm
Kiruna (bucket)	/	Nikon D610 unknown		/

The Canon EOS 70D is used in autofocus mode, whereas the front-station Nikon cameras have a fixed focus according to table Table 3.3.

Table 3.3: Camera settings and specifications.

	Canon EOS 70 D	Nikon D90	Nikon D610
Image sensor	20.2 Mpx	12.3 Mpx	24.3 Mpx
Resolution	5472 px × 3649 px	4288 px × 2848 px	6016 px × 4016 px
Quality	large	fine	fine
Mode & Aperture	A+	A, f/8	A, f/8
ISO	100	200	200
Focal length	Autofocus	17 mm	24 mm

To compare the outputs of both cameras, it is important to know how the camera settings influence the results: The quality parameter controls the compression factor of the stored image, finer quality means larger file size, which leads to a better resolution. The mode of the Nikon camera adjusts the shutter speed and the aperture. In mode A the photographer chooses the aperture and the camera automatically adjusts the shutter speed for optimal exposure. The aperture however, controls the amount of light reaching the image sensor. Low f-numbers increase the size of the aperture and let more light in (adjusted to underground light conditions), whereas high f-numbers decrease the aperture, allowing less light into the camera (www-3, 2018). The Canon camera is used with the scene intelligent auto mode A+, where the camera analyzes the scene and selects all settings automatically to optimize the result. The ISO film speed measures the sensitivity to light exposure. Higher sensitivity leads to a better result in a dark environment and vice versa.

3.1.3 Testing apparatus

The testing apparatus differs depending on the location and the requirements of the image acquisition. All superstructures have the angle of 90° to the investigated surface in common. A fixed distance between the outer left and outer right camera is necessary to scale the DSM. The setups are as follows:

Kiruna front-station

The setup for front-station image acquisition requires four horizontally alligned cameras and consequently four photos of the ROI. The cameras are located at the crown of the excavated drift and moved towards the footwall according to the extraction progress. An illustration of the in situ camera setup and a configuration scheme is shown in Figure 3.1.

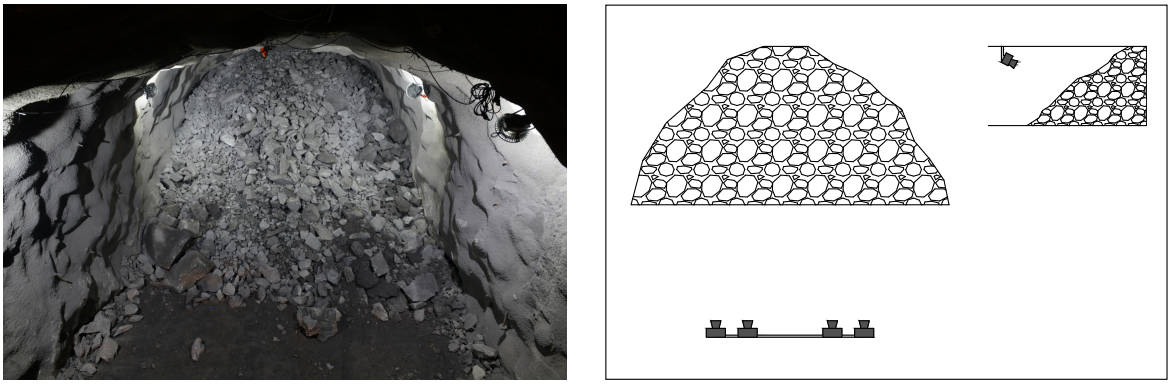

(a) In situ setup (ROI) (b) Scheme

Figure 3.1: Camera setup at front-station.

Kiruna bucket-station

The bucket-station imaging system uses two horizontally aligned cameras to take photos of a passing bucket for DSM generation. The cameras are situated at the crown, but snap orthogonally down at the bucket of a slowly passing LHD (see Figure 3.2).

Figure 3.2: Camera setup at bucket-station (© LKAB).

Laboratory work and simulation

To reproduce the in situ situation as close and flexible as possible, a camera slider with the sliding length of 1.08 m is mounted on a tripod. The slider enables photographs in any number with known distances between the taken images. To guarantee the visibility of the ROI on the 3D image, the overlapping area of all photos is marked (pink tags) at the heap. The sliding setup is shown in Figure 3.3.

Figure 3.3: Camera setup for delineation and FSD validation.

In Table 3.4 the features of the photo recording installations are summarized.

Table 3.4: Testing apparatus characteristics

	Front-station	Bucket-station	Validation setup
Number of photos	4	2	arbitrary
Installation	Crown	Crown	Tripod
Distance of the two outermost cameras	1.40 m	0.35 m	1.08 m

3.2 Software

Two different software packages are used for the DSM generation and the fragmentation measurement. The LKAB Central Control Routine (3GSM, 2018) is used to generate the 3D image via photogrammetry. Pursuing, the BlastMetriX Fragmenter is used for the fragmentation analysis.

3.2.1 LKAB Central Control Routine

The CCR is not only capable of rendering 3D models, it also implements a database function to store, compare and load different image sets and their properties (like camera, their distances etc.). It is customized for the LKAB mining routine and should implement the whole image and fragmentation data in its final state. Testing the functionality of the database is not part of this thesis and is hence not investigated in detail here. The used version for model creation is 1.0.1 (64 bit). The graphical user interface (GUI) of the CCR is illustrated in Figure 3.4.

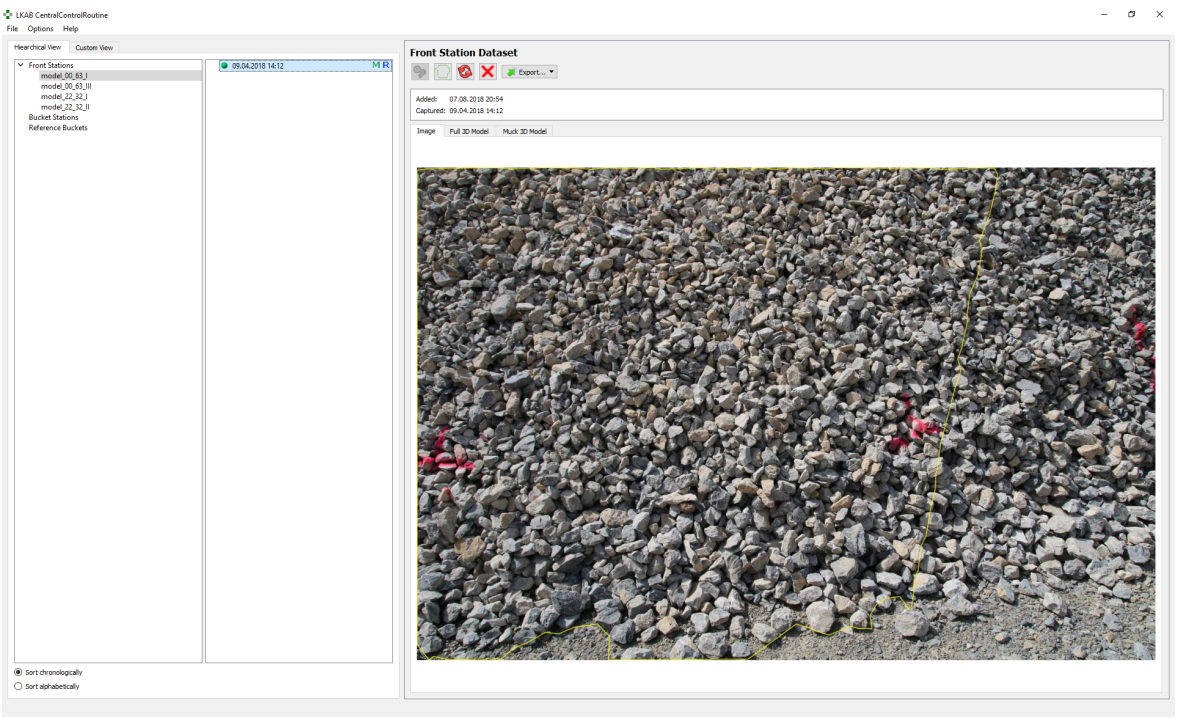

Figure 3.4: GUI of the LKAB CCR.

Input, functionality & output

As mentioned in the previous sections, the LKAB CCR requires at least two photos, with an 100 % overlap of the ROI on all images. Then the photos are loaded into the software, linked together as one set and the distance between the two outermost images is entered. After choosing the ROI at the model or using the automatic muck detection function, the software computes and scales a 3D surface model of the mapped muck pile. The 3D image is then exported as a *.jm3 file, which can be visualized with ShapeMetriX 3D (3GSM, 2018) and imported in the BMX Fragmenter.

3.2.2 BlastMetriX Fragmenter

The BMX Fragmenter is intended to be part of the LKAB CCR at it's final state, but was provided as a stand-alone software in the version 1.0 alpha 5 trunk (64 bit) (see Figure 3.5). The functions of the Fragmenter are more extensive than the CCR's and described hereinafter.

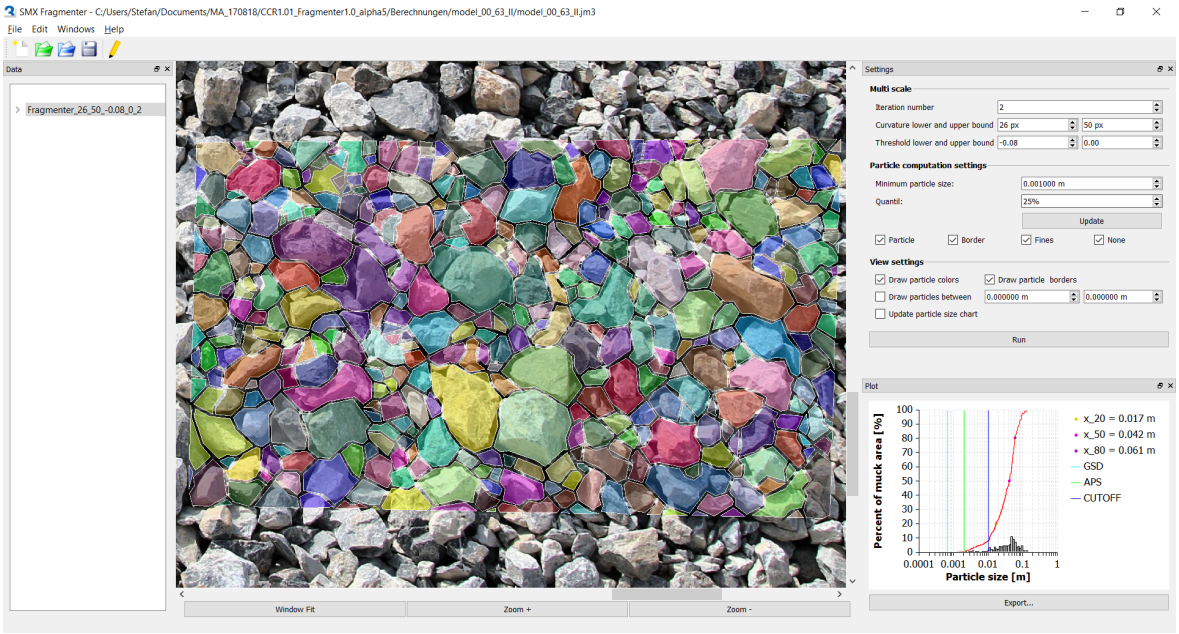

Figure 3.5: GUI of the BMX Fragmenter.

Input, functionality & output

The 3D image, generated by the CCR, serves as input for the BMX Fragmenter. If the automatic muck detection was used in the CCR or the chosen analysis area is still too big, the ROI can be adjusted here. The following parameters are used to control the software's output, but it is yet unknown if all the options will be modifiable in the final version:

Iteration number:

Changes the iterations between the lower and the upper curvature bound. If the iteration number is equal to one, the upper curvature bound is used for the analysis

Curvature lower and upper bound:

Smoothens the boundaries of the detected fragments. A higher smoothing radius leads to thicker edges of the particle. This value is varied within the parameter study.

Threshold lower and upper bound:

Defines the curvature threshold. If the curvature is smaller than the lower bound, a boundary is detected. However, a curvature value above the upper bound indicates a fragment. The standard stocks for this parameter are physically consistent and should not be changed.

Minimum particle size:

Is a cut-off value and changes the region of visible fragment sizes. Values lower than the defined minimum particle size are cropped at the FSD.

Quantil:

Defines the threshold to mark fragments below the defined quantile value.

After the parameter setting, the Fragmenter starts the analysis and displays the FSD as a semi-logarithmic graph. The calculations can be saved for later usage and the grading curve can be exported as a *.csv file. The software implements some visualisation features to highlight detected particles and their borders, show fragments between a certain range and gives information about delineated particles by manual selection. The latest version also includes a mask for manual identification of fines areas and a *Border* function for borderline blocks, which removes fragments that cross the ROI, thereby are possibly cut and do not

represent their actual size. The last very important tool is the display of the ground sampling distance (GSD) and the average point spacing (APS) in the FSD chart. These values are thresholds of the 3D image's resolution (see subsection 2.1.4). The GSD is denoted as the size of one pixel, whereas the APS indicates the average distance of the 3D surface model's point cloud. As it is physically not possible to measure fragments smaller than the size of a pixel and ten pixel match approximately the average distance between two points in the point cloud, no particles smaller than the APS value should be delineated. In this case however, it indicates a malfunction of the software and the model should be recalculated.

Sizing principle

To reproduce a best possible "sieving" result, the BMX Fragmenter implies a novel sizing principle. As mentioned in subsection 2.1.2, 2D fragmentation tools tend to measure the major and intermediate axis of a detected particle, whilst sieving theoretically separates the fragments by their minor and intermediate axis. Through 3D ellipsoid fitting into the muck pile's surface model, the BMX Fragmenter is able to gather all three possible axes of these ellipsoids. After evaluating the minor and intermediate axis of the fitted ellipsoid or ellipsis respectively, the BMX Fragmenter envelopes the smallest possible square around the resulting ellipse, which defines the mesh and thus the size of the delineated fragment (see Figure 3.6).

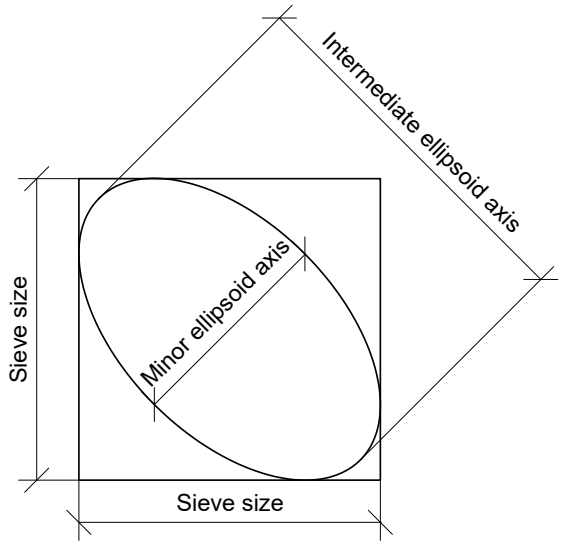

Figure 3.6: Theoretical minimum sieving mesh size of a detected fragment.

3.3 Preliminary assessment and parameter study

To verify the quality of the 3D fragmentation algorithm, a validation sequence is conducted including a parameter study.

Parameter study

One aim of this thesis is to find a robust set of input parameters. To fulfil this requirement, a parameter study regarding the curvature bound is conducted. The study is carried out at the 3D surface models described in Table 3.1 and separated in two stages. Stage one investigates the influence of a coarse variation of the curvature bound on the delineation output, whereas stage two examines the improvement of the resulting FSD confronted with the ground truth by fine adjustment of the curvature intervals. The combination of the results from stage one and two serve as input for stage 2.2 and should lead to the required set of input parameters, to obtain a best possible approximation of the muck pile's grading curve (Table 3.5).

Table 3.5: Parameter study

Stage	Model	Curvature bound	Iterations	Purpose
1	model_00_63_I, model_00_63_II, model_22_32_I, model_22_32_II	01 – 25, 26 – 50, 51 – 75, 76 – 99,	2	Delineation
2.1	model_00_63_I, model_00_63_II, model_22_32_I, model_22_32_II	01 – 25, 26 – 50, 51 – 75, 76 – 99,	2	Delineation & FSD
2.2	model_00_63_I, model_00_63_II	26 – 50	2	Parameter set

3.4 Verification procedure

To quantify and evaluate the algorithm's results, the delineation and the FSD are verified.

3.4.1 Delineation

The validation of the delineation result is conducted based on the parameter study, by visual inspection of the delineated fragments. Following parameters are quantified:

1. The number of detected particles.
2. Disintegrated fragments and count of separated particles responsible for disassociation.
3. Fused fragments and amount of merged particles leading to the conjunction.

To exemplify the results, the relationship between false and true positives is shown in Table 4.1. Thereby, a false positive represents the fusion or disintegration of a fragment, whereas a true positive is a correctly delineated particle.

3.4.2 Fragment Size Distribution

The FSD verification of the BMX Fragmenter is conducted by comparing known grading curves of the limestone quarry in Graz with the computed FSD, using the curvature bound values based on the parameter study. The key parameters for the verification are the x_{20}, x_{50} and the x_{80} values, which correspond to the amount of fragments smaller than 20, 50 respectively 80 % of the maximum particle size. In Table 4.2 the absolute errors Δx_i and the overall error $\sum \Delta x_i$ are shown.

3.5 Application and evaluation of real data

As the BMX Fragmenter is designed for automated fragmentation analysis at the LKAB mine in Kiruna, the algorithm is tested on selected examples, shown in Table 3.1. In the discussion (Chapter 5) the results are checked on plausibility.

4 Results

4.1 Verification procedure based on the parameter study

Herein, the results of the parameter study regarding the muck pile delineation and computed FSD are shown.

4.1.1 Delineation (Stage 1)

To ease and reduce the time for the delineation verification, significant areas of the artificial muck pile's surfaces are chosen and analyzed. For each computed model, the ROI and the resulting delineation with respect to the curvature bound is illustrated according to Table 3.5.

Figure 4.1 shows a well graded muck pile with predominant homogeneous appearance.

(a) model_00_63_I: ROI

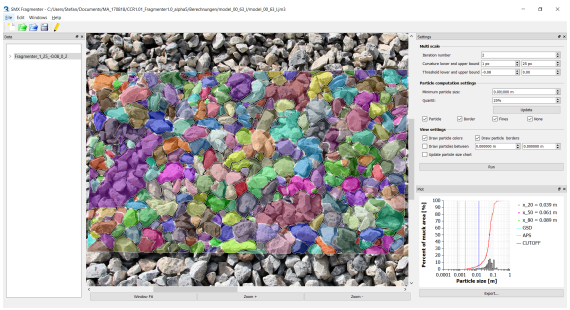

(b) model_00_63_I: 1 – 25 px

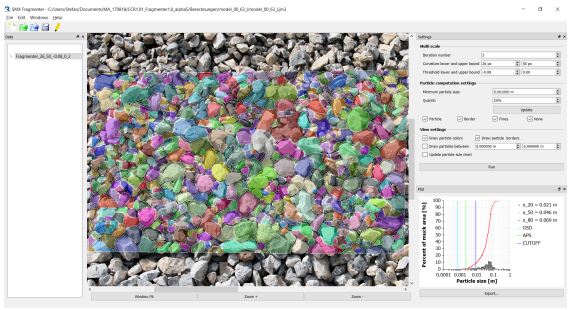

(c) model_00_63_I: 26 – 50 px

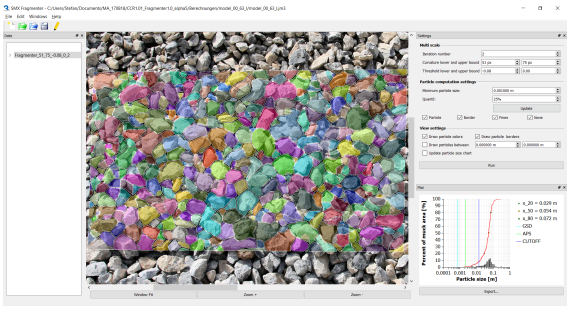

(d) model_00_63_I: 51 – 75 px

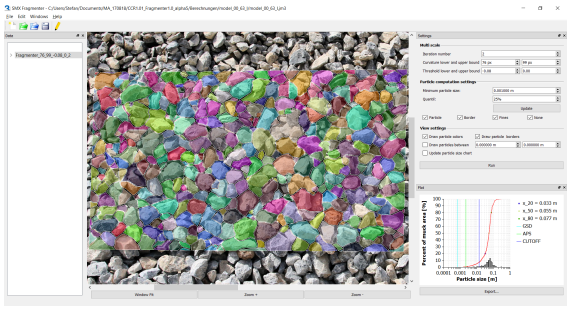

(e) model_00_63_I: 76 – 99 px

Figure 4.1: Delineation, model_00_63_I, stage 1.

A well graded muck pile with rather heterogeneous appearance is illustrated in Figure 4.2

(a) model_00_63_II: ROI

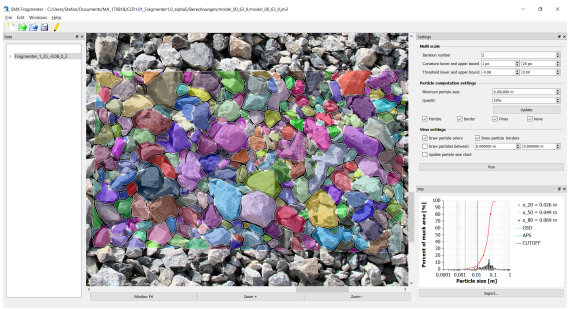

(b) model_00_63_II: 1 – 25 px

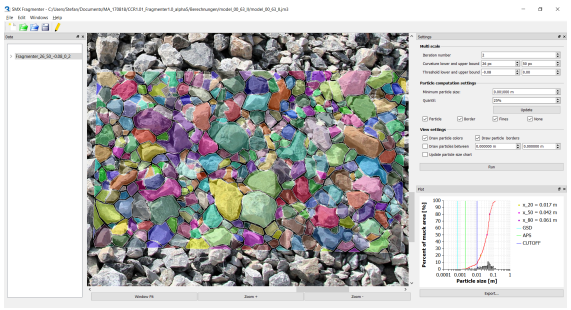

(c) model_00_63_II: 26 – 50 px

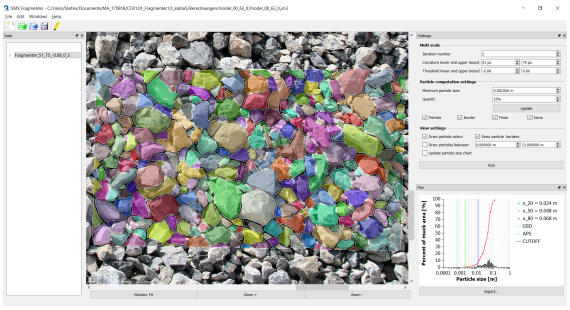

(d) model_00_63_II: 51 – 75 px

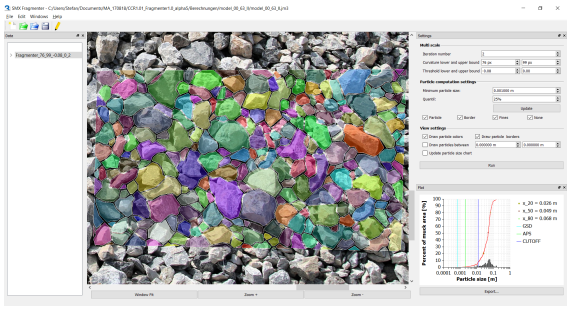

(e) model_00_63_II: 76 – 99 px

Figure 4.2: Delineation, model_00_63_II, stage 1.

Figure 4.3 and Figure 4.4 show close graded muck piles with homogeneous appearance.

(a) model_22_32_I: ROI

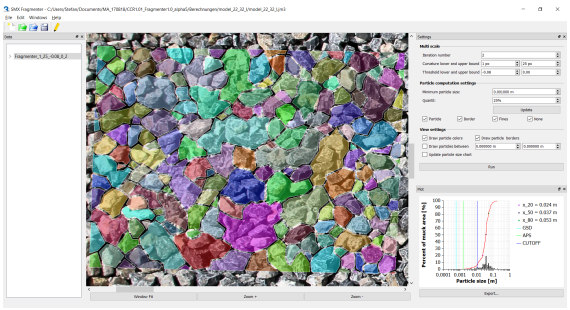

(b) model_22_32_I: 1 – 25 px

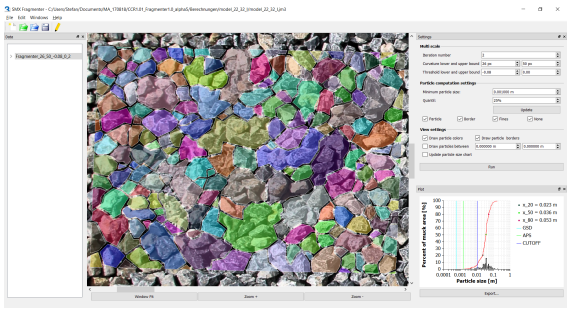

(c) model_22_32_I: 26 – 50 px

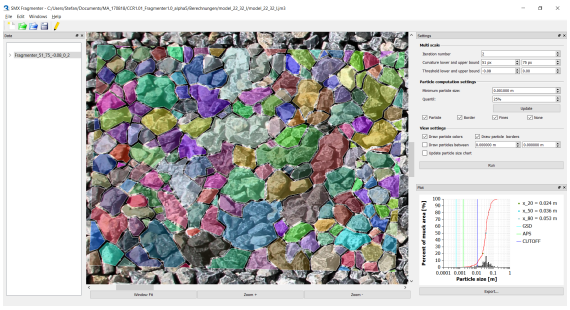

(d) model_22_32_I: 51 – 75 px

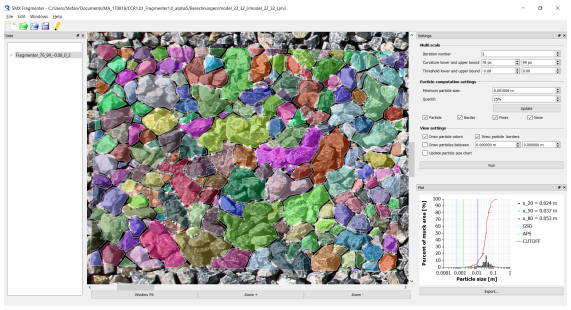

(e) model_22_32_I: 76 – 99 px

Figure 4.3: Delineation, model_22_32_I, stage 1.

(a) model_22_32_II: ROI

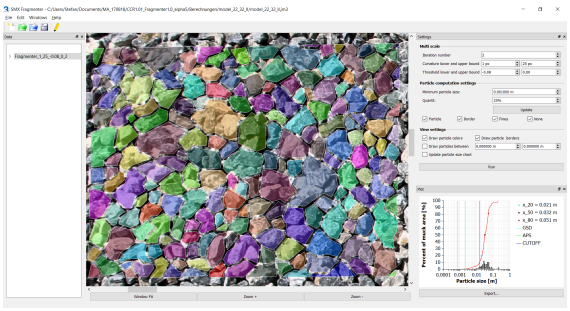

(b) model_22_32_II: 1 – 25 px

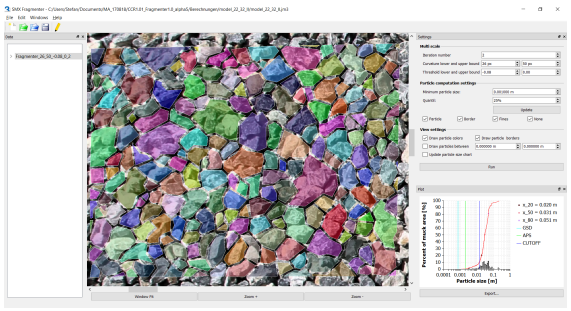

(c) model_22_32_II: 26 – 50 px

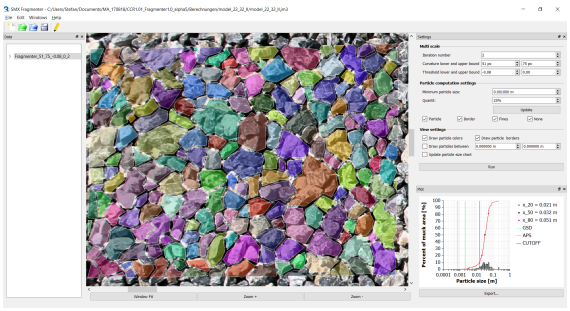

(d) model_22_32_II: 51 – 75 px

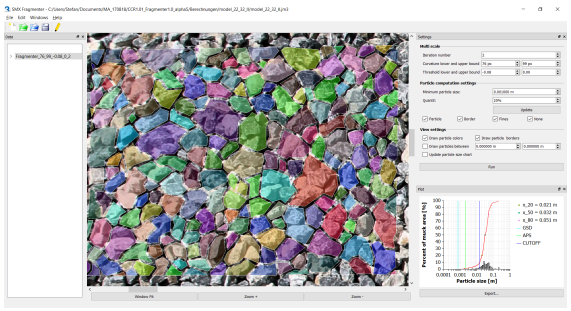

(e) model_22_32_II: 76 – 99 px

Figure 4.4: Delineation, model_22_32_II, stage 1.

An overview of the delineation performance is shown in Table 4.1. The interpretation of the results is exemplified in Chapter 5.

Table 4.1: Delineation verification.

Stage 1						
Model	Curvature bound [px]	$\sum_{Fragm.}$	True positives	False positives		
				Disint.	Fusion	$\sum_{f.posi.}$
00_63_I	01 – 25, 2 It.	306	183 (59.8 %)	35 (11.4 %)	88 (28.8 %)	123 (40.2 %)
00_63_I	26 – 50, 2 It.	419	253 (60.4 %)	115 (27.4 %)	51 (12.2 %)	166 (39.6 %)
00_63_I	51 – 75, 2 It.	405	266 (65.7 %)	57 (14.1 %)	82 (20.2 %)	139 (34.3 %)
00_63_I	76 – 99, 2 It.	384	255 (66.4 %)	38 (9.9 %)	91 (23.7 %)	129 (33.6 %)
00_63_II	01 – 25, 2 It.	257	190 (73.9 %)	16 (6.2 %)	51 (19.8 %)	67 (26.1 %)
00_63_II	26 – 50, 2 It.	301	218 (72.4 %)	47 (15.6 %)	36 (12.0 %)	83 (27.6 %)
00_63_II	51 – 75, 2 It.	280	200 (71.4 %)	28 (10.0 %)	52 (18.6 %)	80 (28.6 %)
00_63_II	76 – 99, 2 It.	278	203 (73.0 %)	14 (5.1 %)	61 (21.9 %)	75 (27.0 %)
22_32_I	01 – 25, 2 It.	185	112 (60.5 %)	10 (5.4 %)	63 (34.1 %)	73 (39.5 %)
22_32_I	26 – 50, 2 It.	190	118 (62.1 %)	14 (7.4 %)	58 (30.5 %)	72 (37.9 %)
22_32_I	51 – 75, 2 It.	191	120 (62.8 %)	10 (5.2 %)	61 (31.9 %)	71 (37.2 %)
22_32_I	76 – 99, 2 It.	190	117 (61.2 %)	11 (5.8 %)	62 (32.6 %)	73 (38.4 %)
22_32_II	01 – 25, 2 It.	205	110 (53.7 %)	6 (2.9 %)	89 (43.4 %)	95 (46.3 %)
22_32_II	26 – 50, 2 It.	220	128 (58.2 %)	11 (5.0 %)	81 (36.8 %)	92 (41.8 %)
22_32_II	51 – 75, 2 It.	214	111 (51.9 %)	10 (4.6 %)	93 (43.5 %)	103 (48.1 %)
22_32_II	76 – 99, 2 It.	210	110 (52.4 %)	10 (4.7 %)	90 (42.9 %)	100 (47.6 %)

4.1.2 Fragment Size Distribution (Stage 2)

In contrast to stage one (subsection 3.4.1), the whole muck pile serves as input for the FSD computation at stage two. To get valid results, it is necessary to analyze the whole fragment heap to eliminate the influence of the chosen ROI on the grading curve as best as possible.

Table 4.2: FSD verification before fine-tuning of the curvature bound.

Stage 2.1					
Model	Curvature bound [px]	Error Δx_i [mm]			$\sum \Delta x_i$[mm]
		Δx_{20}	Δx_{50}	Δx_{80}	
00_63_I	01 – 25, 2 It.	35.18	36.48	40.70	112.36
00_63_I	26 – 50, 2 It.	20.49	26.99	25.39	72.87
00_63_I	51 – 75, 2 It.	28.83	31.00	29.37	89.20
00_63_I	76 – 99, 2 It.	30.94	33.04	31.60	95.58
00_63_II	01 – 25, 2 It.	19.44	20.49	25.11	65.04
00_63_II	26 – 50, 2 It.	12.02	9.82	8.52	30.36
00_63_II	51 – 75, 2 It.	15.73	14.53	11.52	41.78
00_63_II	76 – 99, 2 It.	16.98	16.51	14.43	47.93
22_32_I	01 – 25, 2 It.	0.45	8.05	22.81	31.31
22_32_I	26 – 50, 2 It.	1.62	7.05	21.50	30.17
22_32_I	51 – 75, 2 It.	0.95	7.35	20.98	29.27
22_32_I	76 – 99, 2 It.	0.67	7.62	21.86	30.15
22_32_II	01 – 25, 2 It.	1.99	6.06	21.56	29.61
22_32_II	26 – 50, 2 It.	3.27	4.90	19.39	27.56
22_32_II	51 – 75, 2 It.	2.48	5.31	19.67	27.46
22_32_II	76 – 99, 2 It.	2.30	5.60	19.88	27.77

After examination of the overall error $\sum \Delta x_i$ in combination with the delineation ratio $\sum_{f.posi.}$, the parameter set according to Table 4.3 undergoes further investigation. Due to the small differences in the overall FSD error of model_22_32_I and model_22_32_II ($\pm\,1.1$ mm), they are not considered in the further analysis.

Table 4.3: Curvature fine-tuning stage 2.2.

Stage	Model	Curvature bound [px]	Iterations	Purpose
2.2	model_00_63_I, model_00_63_II	26 – 32 33 – 38 39 – 44 45 – 50	2	Parameter set

The fine adjustment of the curvature bound shows slight improvement and the results are illustrated in Table 4.4.

Table 4.4: FSD verification after fine-tuning of the curvature bound.

Stage 2.2					
Model	Curvature bound [px]	Error Δx_i [mm]			$\sum \Delta x_i$[mm]
		Δx_{20}	Δx_{50}	Δx_{80}	
00_63_I	26 – 32, 2 It.	19.88	25.57	24.93	70.38
00_63_I	33 – 38, 2 It.	22.37	28.00	26.79	77.17
00_63_I	39 – 44, 2 It.	25.03	29.25	28.34	82.61
00_63_I	45 – 50, 2 It.	27.40	30.24	28.70	86.34
00_63_II	26 – 32, 2 It.	11.69	9.39	7.58	28.65
00_63_II	33 – 38, 2 It.	13.42	10.86	9.18	33.47
00_63_II	39 – 44, 2 It.	14.29	12.49	10.24	37.02
00_63_II	45 – 50, 2 It.	15.01	13.44	10.35	38.81

4.2 Application and evaluation of real data

Figure 4.5 shows the ROI and the delineation result of a muck pile (front-station) from the Kiruna LKAB underground mine.

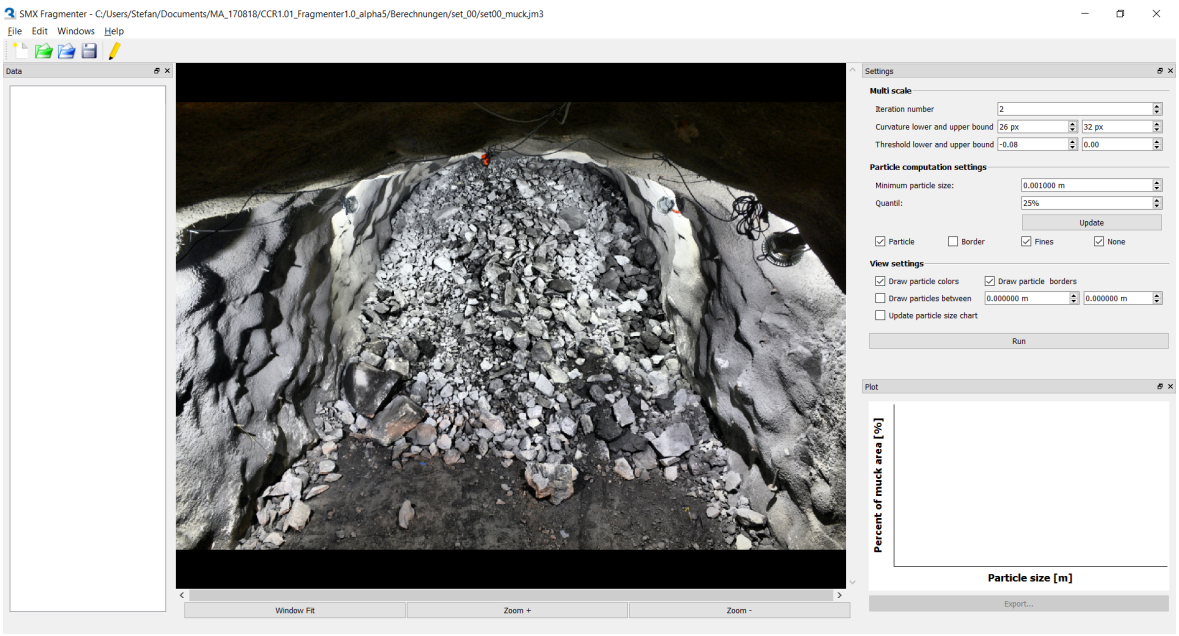

(a) set_00: ROI

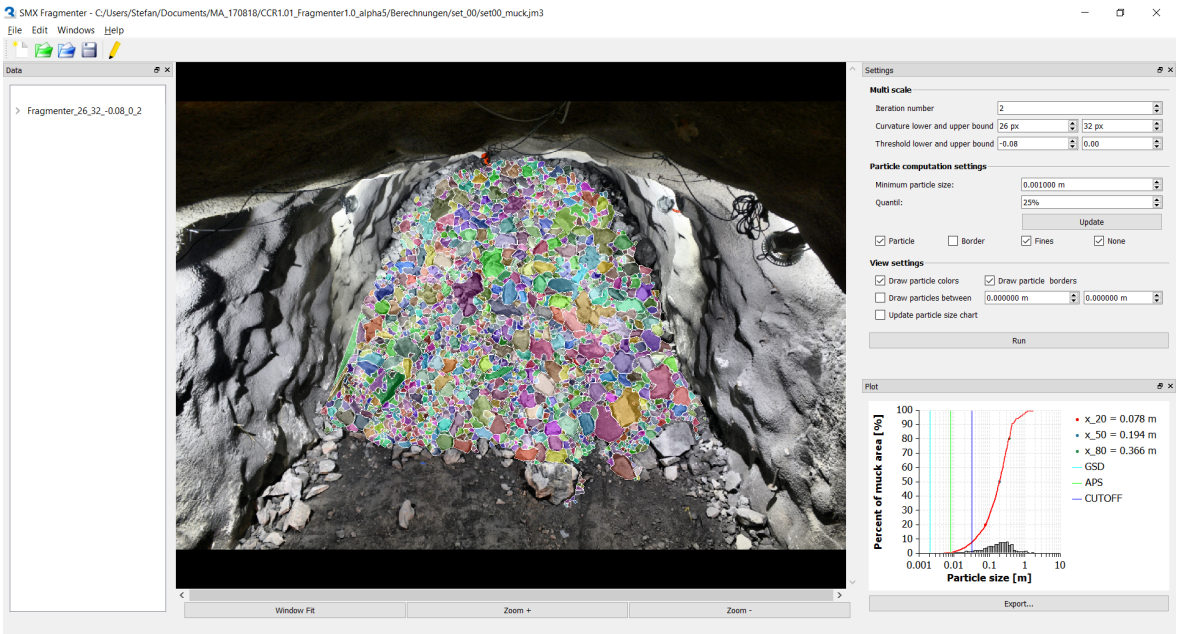

(b) set_00: 26 – 32 px

Figure 4.5: Delineation, set_00, real data.

The ROI and the delineated bucket of a LHD are illustrated in Figure 4.6

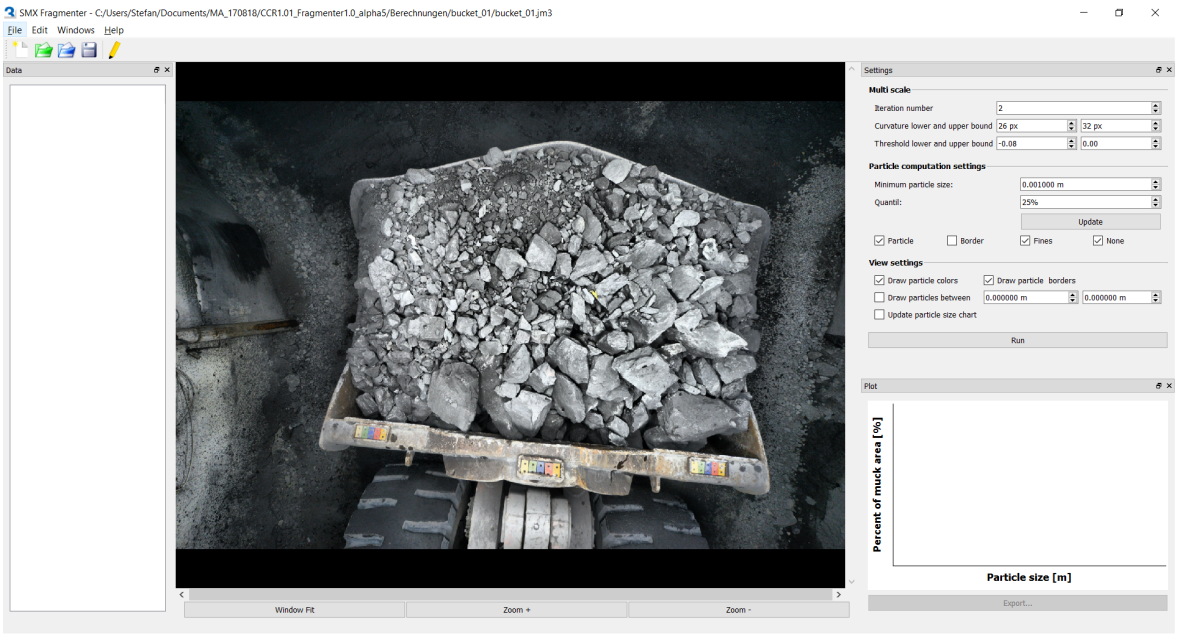

(a) bucket_01: ROI

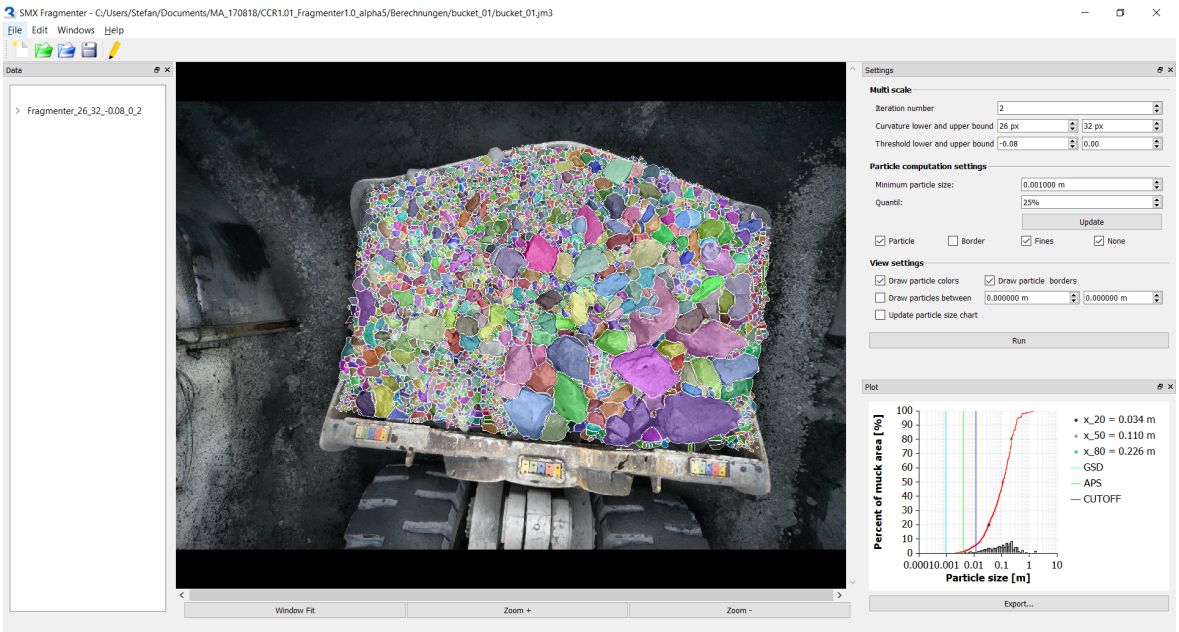

(b) bucket_01: 26 – 32 px

Figure 4.6: Delineation, bucket_01, real data.

5 Discussion

5.1 Verification procedure

5.1.1 Delineation (Stage 1)

The well graded model_00_63_I shows noticeable improvement of the delineation performance with increasing curvature values. At lower and interestingly also upper curvature bounds, the predominant misidentification refers to the fusion of adjacent fragments ($\sim 24\,\%$). This leads to some extent to an overestimation of the actual block size. From $26-50\,\mathrm{px}$ the dominant misidentification changes to disintegration phenomena. In general, false positives tend to appear in groups. Model_00_63_II behaves very similar to model_00_63_I, misidentification according to fusion decreases from 19.8 % to 12.0 % at the curvature bound from $26-50\,\mathrm{px}$, prior to increasing up to 21.9 % again at the last calculation interval. It must be stated that model_00_63_II has a much lower, almost constant, false positive rate of about 27 %.

The poorly graded model_22_32_I shows a considerable constant false positive rate over all calculation intervals of about 38 %. The predominant misidentification feature is fusion. Disintegration phenomena are rare, compared to the coarser models and almost constant with roughly 6 %. Model_22_32_II shows an even lower disintegration rate with about 4 %. On the other hand, the overall false positive rate increases significantly to approximately 46 %. Only from $26-50\,\mathrm{px}$ the DSM presents an improved false delineation ratio, similar to model_22_32_I with 42 %.

In Table 4.1, the influence of the muck pile's grading on the particle delineation is displayed. Well graded heaps tend to deliver optimal results at higher curvature bounds during the executed investigation, while poor graded muck piles show the best delineation result at lower or intermediate curvature levels. Small particles are most likely merged to one fragment, whereas big blocks tend to be disintegrated into smaller particles, depending on the curvature setting. In general, the BMX Fragmenter tends to fuse particles instead of disassociating

them. It is hard to define a generic behaviour of the algorithm regarding disintegration or fusion of medium size blocks though. In some cases separation prevails, in other cases fusion occurs. Consequently, additional knowledge about the FSD of the delineated muck piles is necessary to make a reliable statement about the appropriate curvature bound setting for a variety of fragmentation scenarios.

5.1.2 Fragment Size Distribution (Stage 2)

In addition to the delineation analysis, FSD for the different curvature bound settings are presented herein to visualize the BMX Fragmenters approximation of the ground truth. The curvature intervals and the absolute error of the sieve passing parameters x_i are shown in Table 4.2.

The FSD of model_00_63_I at stage 2.1 (Figure 5.1) shows a rough approximation to the ground truth drawn in black. The curvature bound of 26 – 50 px is the best fit to the actual grading curve with a $\sum \Delta x_i$ value of about 73 mm. Although, the fragments are measured twice their size on average, the shape of the computed FSD approaches the ground truth fairly well.

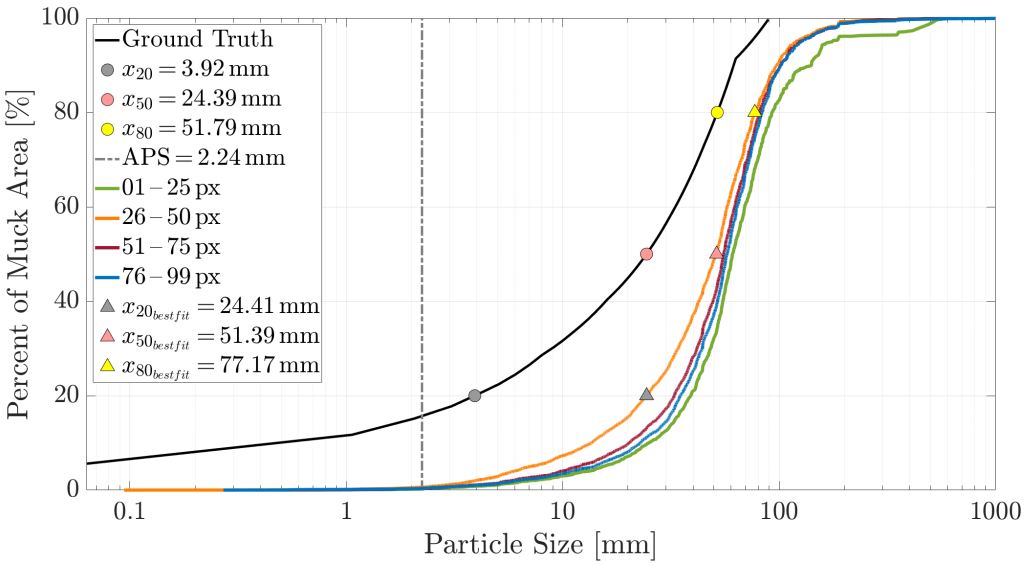

Figure 5.1: FSD, model_00_63_I, stage 2.1.

Figure 5.2 displays the FSD of model_00_63_II. It it obvious, that the model represents the ground truth much better than model_00_63_I. The overall error decreases to 30 mm, which represents a average sizing ratio of about 1.4:1, compared to the ground truth. Again, a

curvature bound of 26 – 50 px results in the best fit. In the upper part, the FSD converges towards the ground truth, whereas the fine particle share is underestimated.

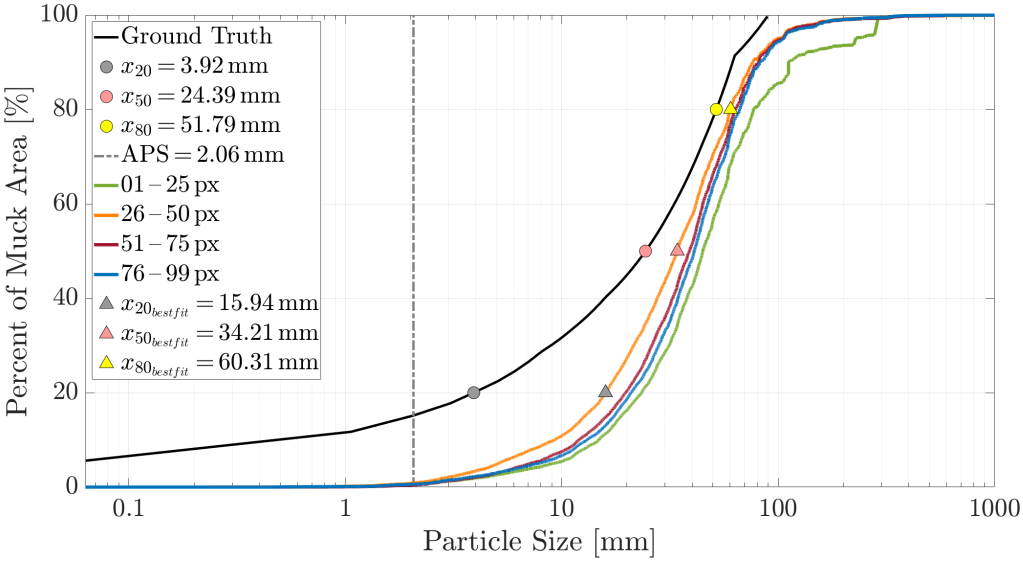

Figure 5.2: FSD, model_00_63_II, stage 2.1.

Model_22_32_I exhibits almost no change of particle sizes due to curvature variation. Figure 5.3 shows a consistent FSD for all curvature intervals. The best approximation is achieved with a curvature bound of 51 – 75 px though. The x_{20} value is met almost perfectly with an error of about 1 mm, whereas x_{50} and x_{80} display a magnification of 1.3:1, respectively 1.7:1.

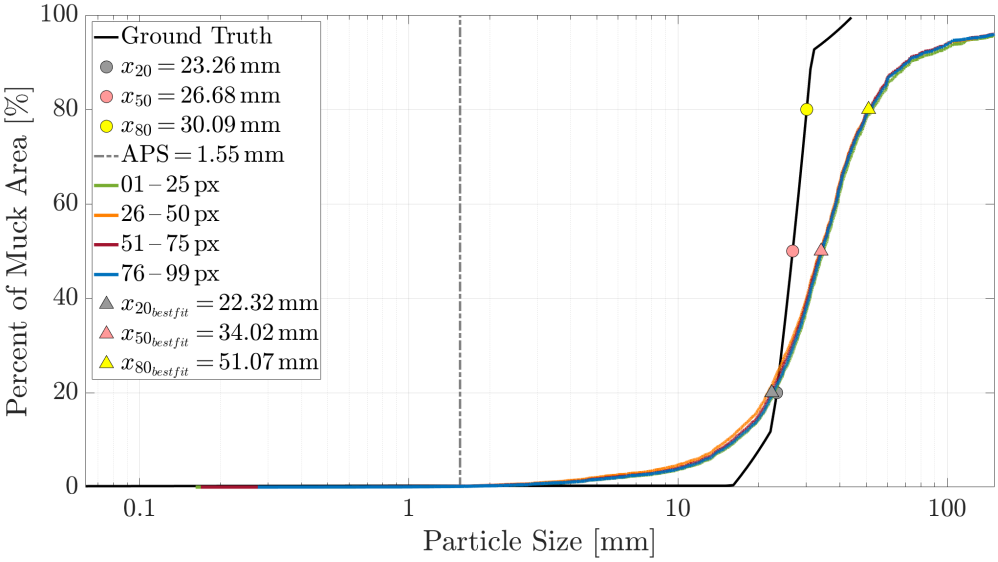

Figure 5.3: FSD, model_22_32_I, stage 2.1.

Model_22_32_II (Figure 5.4) depicts nearly the same representation of the 22/32 mm muck pile as model_22_32_I. The FSD fits the lower part of the ground truth well, with a downsizing regarding x_{20} of 0.9:1 and an enlargement at x_{50} of about 1:1.2. Δx_{80} decreases compared to model_22_32_I around 6 % to 19.67 mm.

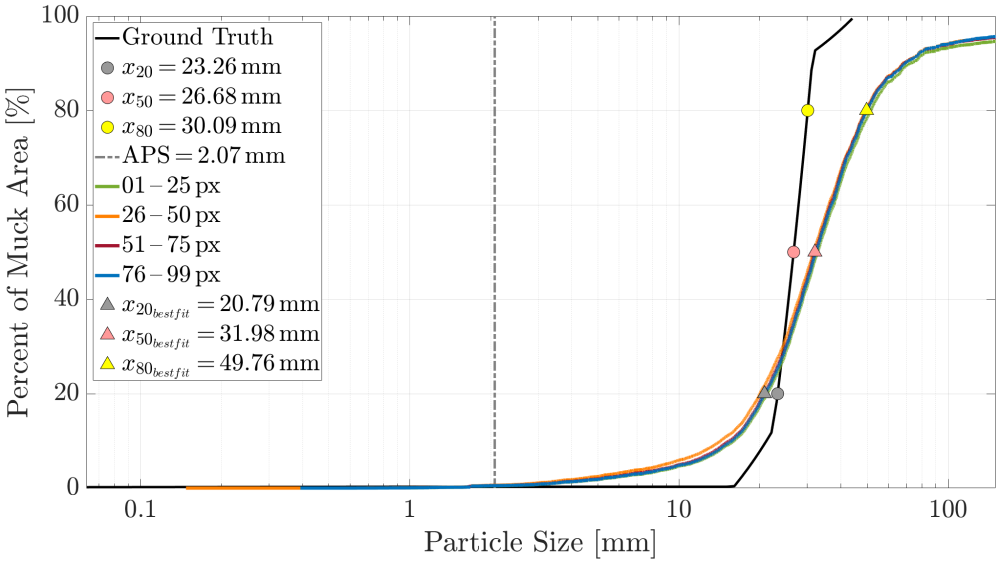

Figure 5.4: FSD, model_22_32_II, stage 2.1.

Considering the FSD results of all four surface models under varying curvature bound iterations, a distinction must be made between close and wide graded muck piles. Although, they have similar curvature ranges for the best possible fragmentation measurement (26 – 75 px), their fit to the ground truth distinguishes clearly. The 22/32 mm DSM show the best approximations at small fragment sizes, whereas the 0/63 mm models converge with greater particle sizes towards the ground truth. A parameter set, combining a closer fit at both regions, could not be identified by changing the curvature settings alone. Analyzing both, the delineation and the FSD results of the BMX Fragmenter, unfortunately does not deliver an explicit curvature bound for optimal fragmentation analysis. Most commonly, where the delineation ratio is at its maximum, the approximation of the FSD to the ground truth achieves just a moderate level and vice versa. The juxtaposition of the true positive ratio and the overall error ($\sum \Delta x_i$) shows the best combination, of a minor false positive ratio, with a low overall error, at the curvature interval 26 – 50 px. Consequently, this curvature bound is used for the fine-tuning of the FSD approximation at stage 2.2.

Figure 5.5 displays the benefit of fine-tuning the curvature range. The improvement is small ($\sim 3\,\%$), but maximizes as presumed, with Δx_{50} decreasing from 26.99 to 25.57 mm and Δx_{20} reducing about 0.6 mm.

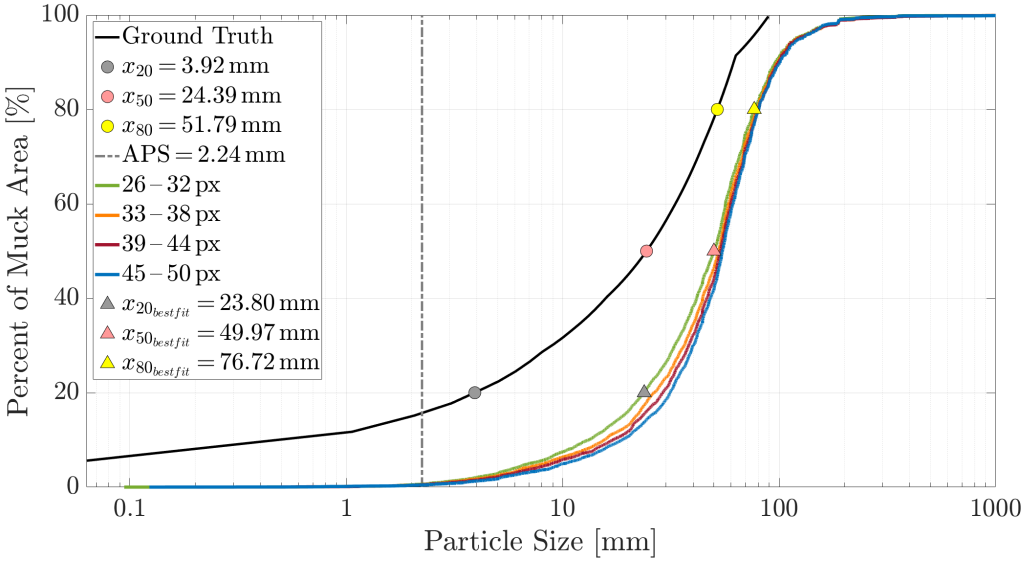

Figure 5.5: FSD, model_00_63_I, stage 2.2.

Model_00_63_II inherently approximates the 0/63 mm muck pile better and shows roughly 6 % enhancement due to small-scale curvature iteration.

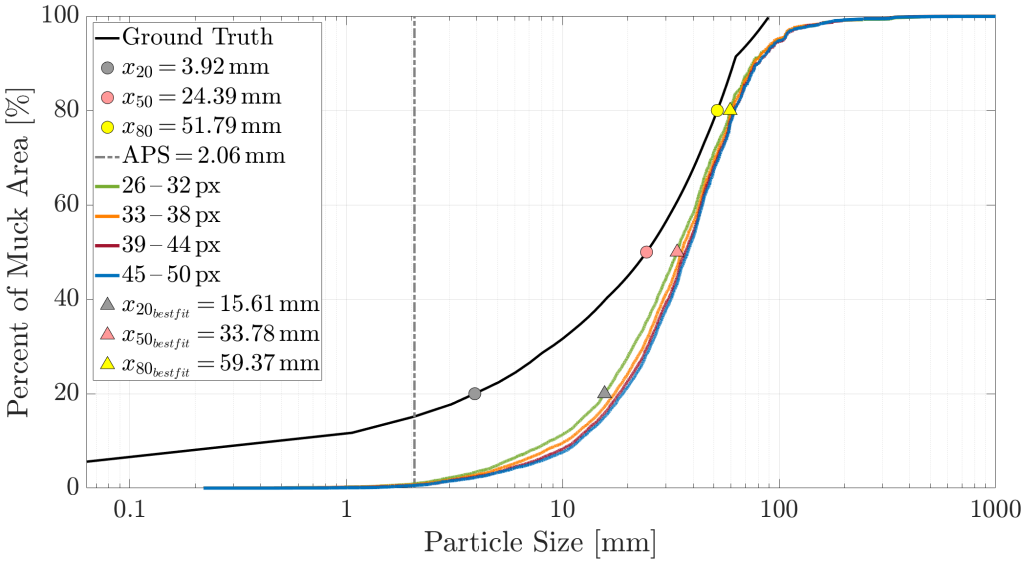

Figure 5.6: FSD, model_00_63_II, stage 2.2.

5.2 Application and evaluation of real data

Figure 5.7 illustrates the FSD of set_00, aquired by the front-station camera setup. There is little to say about the quality of the approximated grading curve. However, considering the delineation of the muck pile, the result looks plausible. The algorithm works fine on real data, behaves very similar to the tested muck piles and shows a good delineation result. Two bigger blocks at the lower left are disintegrated and there seems to be the tendency to consolidate fragments in the muck pile center. The border fragments were cropped, which results in the non-detection of some boundary blocks (Figure 4.5b).

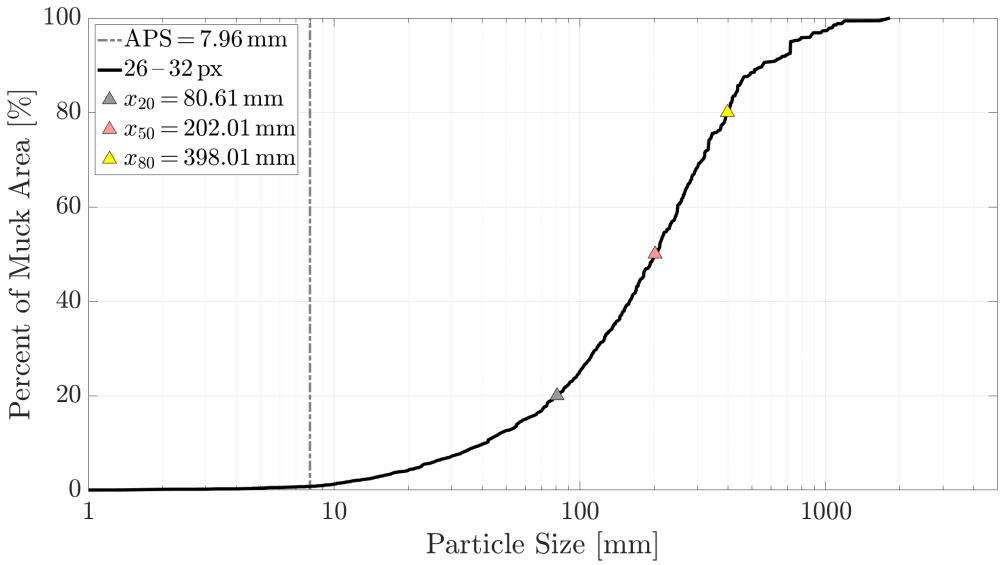

Figure 5.7: FSD, set_00, real data.

The bucket station investigation visible in Figure 5.8 shows a very similar result as the front-station setup. The FSD looks reasonable and despite the disassociation of two larger blocks and the boundary artefacts, due to the bucket/bottom transition, the delineation looks good. The algorithm is capable to detect seven fragments lying on a bigger block right next to the bucket center (Figure 4.6b). This indicates the robust delineation effort associated with BMX Fragmenter.

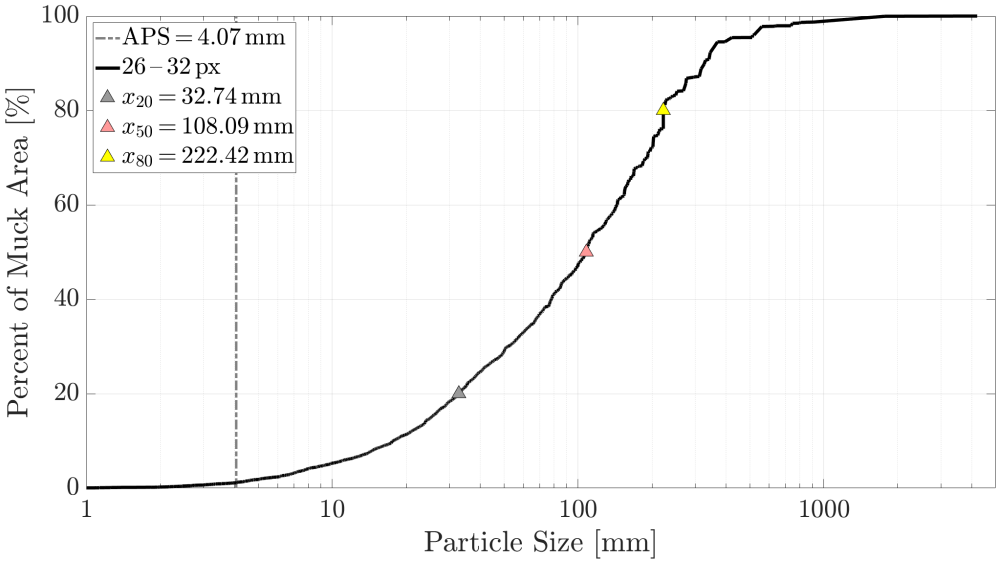

Figure 5.8: FSD, bucket_01, real data.

Unfortunately, there is no front- respectively bucket station data available, which originates from one muck pile. The consecutive analysis of front- and bucket station DSM after successive LHD draw, could provide first insightful information about the resemblance of the computed FSD, without the effort of sieving.

It remains to be seen whether both imaging stations will survive. The bucket station seems to be the better fragmentation monitoring solution, due to its preferable applicability and integration in the daily mining routine. The installation at a LHD reversal point on the way to the ore pass, allows a smooth work flow during the ore draw. In contrast, the front station must be moved along the drift, depending on the extraction advance. In any case, further research regarding the BMX Fragmenters practical applicability must be coordinated with future plans of underground image acquisition.

6 Conclusion and Outlook

This thesis presents the newly designed 3D fragmentation algorithm implemented in the BMX Fragmenter and is intended to establish the software for fragmentation analysis. After conducting a series of tests on DSM of muck piles with various FSD and fragment arrangement, the main conclusions are presented by answering the elaborated research questions.

Is the fragment delineation plausible regarding the number of false positives and true negatives?

With an average degree of true positives of 62.9 % and respectively 37.1 % false positives amongst all computations, the BMX Fragmenter's delineation output provides satisfactory evidence of the software's functionality regarding particle delineation at its current development state. All calculations were conducted fully automated and without any post-processing of the delineation results. With outliers in both directions, in other words, with a minimum true positive ratio of 51.9 % and a maximum true positive percentage of 73.9 %, the possible range of correct delineated particles of an automated fragmentation logic become visible.

Withstands the obtained FSD of the algorithm a verification by known grading curves from artificial muck piles?

As the tests have shown, the gathered FSD is highly dependent on the DSM and further on the heap itself. The investigated muck piles distinguish in particle size, appearance, as well as sampling area. Consequently, different fragment sizes, grading properties and investigation areas deliver different FSD results. All in all, the computed FSD delivers a good impression of the actual grading curve. There are some critical regions (over estimation of the FSD around x_{20}, resp. x_{80}), depending on the DSM, which are associated with the tendency of the algorithm to fuse particles. The trend of merging particles was already noticeable during the delineation verification, but is confirmed as well after the FSD survey.

What are the software's limitations at the current state and what is possible regarding the 3D fragmentation algorithm in the future?

Like other fragmentation measurement software, the BMX Fragmenter has slight problems with small particle delineation. The *Border* function for the removal of borderline blocks, visualizes the changing FSD, but does not update the corresponding *.csv output file. Sometimes, if the ROI is chosen too generous, the boundary blocks and the surrounding area of the muck pile merge and are delineated as one big fragment. As experience teaches, the cropping of those blocks with the *Border* tool could reduce the overall error significantly. The mentioned fusion of multiple fragments and the particle/surrounding consolidation lead to an overestimation of the FSD and generate a visible offset compared to the ground truth. In future surveys, blasted material could be sieved and used for a verification of the in situ FSD. This could provide valuable insight into the possible application scenarios at the LKAB underground mines.

Considering possible developments, future releases may implement a fragmentation prediction tool, covering the full range of blasting, starting at the blast design, continuing with fragmentation measurement and ending with the prediction of possible fragmentation scenarios, based on previous blast data. Maybe that is a little too far ahead, so pursuing the development, the fragmentation algorithm must be continuously tested in its further stages to improve the delineation result and approximate the ground truth by the computed FSD as accurately as possible.

A comparison with the industry standard Split-Desktop (Split Engineering, 2010) is the very next step during testing the BMX Fragmenter. The results are published in a subsequent report and will provide revealing insight into the software's possible position on the market.

Bibliography

Cokayne, E. (1982). Sublevel Caving: An Introduction. In R. Gertsch & R. Bullock (Eds.), *Techniques in Underground Mining* chapter 4, (pp. 605–619). Society for Mining, Metallurgy, and Esploration, Inc.

Eden, D. & Franklin, J. (1996). Disintegration, fusion and edge net fidelity. In *Proceedings of the FRAGBLAST 5, Workshop on Measurement of Blast Fragmentation*, (pp. 127–132).

Gaich, A., Pötsch, M., Moser, P., & Schubert, W. (2010). How 3D images support bench face profiling, blast planning and rock mass characterisation. In *Proceedings of the 9th International Symposium on Rock Fragmentation by Blasting*, (pp. 85–90).

Han, J. & Song, J. (2014). Statistical estimation of blast fragmentation by applying stereophotogrammetry to block piles. *International Journal of Rock Mechanics and Mining Sciences*, *68*, 150–158.

Kvapil, R. (1998). The Mechanics and Design of Sublevel Caving Systems. In R. Gertsch & R. Bullock (Eds.), *Techniques in Underground Mining* chapter 4, (pp. 621–653). Society for Mining, Metallurgy, and Esploration, Inc.

Maerz, N., Palangio, T., & Franklin, J. (1996). WipFrag Image Based Granulometry System. In *Proceedings of the FRAGBLAST 5 Workshop on Measurement of Blast Fragmentation*, (pp. 91–99).

Maerz, N. & Zhou, W. (1998). Optical digital fragmentation measuring systems - inherent sources of error. *FRAGBLAST, The International Journal for Blasting and Fragmentation*, *4*(4), 415–431.

Noy, M. (2013). Automated rock fragmentation measurement with close range digital photogrammetry. In *Proceedings of the FRAGBLAST 10, Workshop on Measurement and Analysis of Blast Fragmentation*, (pp. 13–21).

Rhigetti, E. (2014). 2D Fragmentation analysis of Sublevel Caving ring blasts. Measurements based on front and bucket images using SplitDesktop. Master's thesis, University of Trento.

Rustan, R., Cunningham, C., Fourney, W., Simha, K., & Spathis, A. (2011a). Fragment Size Distribution. In *Mining and Rock Construction Technology Desk Reference* chapter 4, (pp. 181). CRC Press/Balkema.

Rustan, R., Cunningham, C., Fourney, W., Simha, K., & Spathis, A. (2011b). Fragmentation. In *Mining and Rock Construction Technology Desk Reference* chapter 4, (pp. 179). CRC Press/Balkema.

Sanchidrián, J., Segarra, P., & López, L. (2005). A Practical Procedure for the Measurement of Fragmentation by Blasting by Image Analysis. *Rock Mechanics and Rock Engineering*, *39*, 359–382.

Sanchidrián, J., Segarra, P., Ouchterlony, F., & López, L. (2008). On the accuracy of fragment size measurement by image analysis in combination with some distribution functions. *Rock Mechanics and Rock Engineering*, *42*, 95–116.

Split Engineering, L. (2016). *Split-Desktop Version 4, Help Manual.* Tucson, AZ 85745 USA: Split Engineering, LLC.

Thurley, M., Wimmer, M., & Nordqvist, A. (2015). Blast fragmentation measurement based on 3D imaging in sublevel caving draw-points and LHD buckets at LKAB Kiruna. In *Proceedings of the 11th International Symposium on Rock Fragmentation by Blasting*, (pp. 1–17).

Wimmer, M. (2017). Sublevel Caving. Lecture notes.

www-1 (2018). Sublevel Caving Mining Method. `https://www.youtube.com/watch?v=-9BDHl_acrU`. Accessed: 2018-04-22.

www-2 (2018). Our underground mines. `https://www.lkab.com/en/about-lkab/from-mine-to-port/mining/our-underground-mines`. Accessed: 2018-07-20.

www-3 (2018). Aperture. `https://imaging.nikon.com/support/digitutor/d3300/functions/aperture.html`. Accessed: 2018-08-04.